Journal of Geophysical Research: Oceans

RESEARCH ARTICLE
10.1029/2018JC014059

Special Section:
The Southern Ocean Carbon and Climate Observations and Modeling (SOCCOM) Project: Technologies, Methods, and Early Results

Southern Ocean Biogeochemical Float Deployment Strategy, With Example From the Greenwich Meridian Line (GO-SHIP A12)

L. D. Talley[1], I. Rosso[1], I. Kamenkovich[2], M. R. Mazloff[1], J. Wang[3], E. Boss[4], A. R. Gray[5], K. S. Johnson[6], R. M. Key[7], S. C. Riser[5], N. L. Williams[8,9], and J. L. Sarmiento[7]

[1]Scripps Institution of Oceanography, University of California, San Diego, La Jolla, CA, USA, [2]Rosenstiel School of Marine and Atmospheric Sciences, University of Miami, Miami, FL, USA, [3]Jet Propulsion Laboratory, California Institute of Technology, Pasadena, CA, USA, [4]School of Marine Sciences, University of Maine, Orono, ME, USA, [5]School of Oceanography, University of Washington, Seattle, WA, USA, [6]Monterey Bay Aquarium Research Institute, Moss Landing, CA, USA, [7]Program in Atmospheric and Oceanic Sciences, Princeton University, Princeton, NJ, USA, [8]College of Earth, Ocean, and Atmospheric Sciences, Oregon State University, Corvallis, OR, USA, [9]Now at Pacific Marine Environmental Laboratory, National Oceanic and Atmospheric Administration, Seattle, WA, USA

Key Points:
- SOCCOM float deployment strategy is based on prior water mass, frontal zone, forcing, and circulation information from data and models
- These floats were deployed in the sea ice zone, Weddell and Ross Seas, Antarctic Circumpolar Current, and Subantarctic and Subtropical Zones
- Floats have already provided information on carbon outgassing, mixing during Maud Rise polynya, oxygen utilization, and net community production

Supporting Information:
- Supporting Information S1

Correspondence to:
L. D. Talley,
ltalley@ucsd.edu

Citation:
Talley, L. D., Rosso, I., Kamenkovich, I., Mazloff, M. R., Wang, J., Boss, E., et al. (2019). Southern Ocean biogeochemical float deployment strategy, with example from the Greenwich Meridian line (GO-SHIP A12). *Journal of Geophysical Research: Oceans*, *124*, 403–431. https://doi.org/10.1029/2018JC014059

Received 13 APR 2018
Accepted 21 SEP 2018
Accepted article online 28 SEP 2018
Published online 21 JAN 2019

The copyright line for this article was changed on 28 JAN 2019 after original online publication.

Abstract Biogeochemical Argo floats, profiling to 2,000-m depth, are being deployed throughout the Southern Ocean by the Southern Ocean Carbon and Climate Observations and Modeling program (SOCCOM). The goal is 200 floats by 2020, to provide the first full set of annual cycles of carbon, oxygen, nitrate, and optical properties across multiple oceanographic regimes. Building from no prior coverage to a sparse array, deployments are based on prior knowledge of water mass properties, mean frontal locations, mean circulation and eddy variability, winds, air-sea heat/freshwater/carbon exchange, prior Argo trajectories, and float simulations in the Southern Ocean State Estimate and Hybrid Coordinate Ocean Model (HYCOM). Twelve floats deployed from the 2014–2015 Polarstern cruise from South Africa to Antarctica are used as a test case to evaluate the deployment strategy adopted for SOCCOM's 20 deployment cruises and 126 floats to date. After several years, these floats continue to represent the deployment zones targeted in advance: (1) Weddell Gyre sea ice zone, observing the Antarctic Slope Front, and a decadally-rare polynya over Maud Rise; (2) Antarctic Circumpolar Current (ACC) including the topographically steered Southern Zone *chimney* where upwelling carbon/nutrient-rich deep waters produce surprisingly large carbon dioxide outgassing; (3) Subantarctic and Subtropical zones between the ACC and Africa; and (4) Cape Basin. Argo floats and eddy-resolving HYCOM simulations were the best predictors of individual SOCCOM float pathways, with uncertainty after 2 years of order 1,000 km in the sea ice zone and more than double that in and north of the ACC.

Plain Language Summary The Southern Ocean, which surrounds Antarctica, is a huge, very sparsely observed region. But we know from the decades of observations and from computer models that the Southern Ocean is a major player in the Earth's climate, taking up a significant fraction of the excess carbon dioxide from the atmosphere and absorbing a large fraction of the extra heat that results from that extra carbon dioxide. The extra carbon dioxide is also acidifying the Southern Ocean waters. To observe these, we are expanding one of the major ocean-observing systems: *Argo* profiling floats that measure temperature and salinity to 2,000-m depth every 10 days. SOCCOM has (1) added extra sensors that measure the ocean's pH, oxygen, nitrate, chlorophyll, and particles; (2) developed algorithms to derive the rest of the carbon budget terms, and (3) vigorously expanded Argo into the enormous seasonal ice zone. We are deploying about 30 floats per year all around Antarctica. We describe our strategy for float deployments in 2014 in the large region between Africa and Antarctica, describing the circulation, water properties, and forcing of this region. We evaluate how well we met our goal of sampling each of the distinct oceanographic regimes.

1. Introduction

The Southern Ocean Carbon and Climate Observations and Modeling (SOCCOM) experiment, which began in 2014, was developed to improve understanding and representation of the global carbon and heat budgets and air-sea exchanges in coupled climate models. In formulating SOCCOM, it was appreciated that measuring and understanding regional Southern Ocean processes is central to model improvement and that the overwhelming lack of in situ observations, especially those that resolve seasonal cycles within the

extensive ice-covered regions, has impeded progress (Frölicher et al., 2015; Russell et al., 2018). Geographically diverse processes within SOCCOM's very large region include, among others, air-sea carbon fluxes and budgets (Gray et al., 2018; Takahashi et al., 2009), biological processes (Ardyna et al., 2017; Arteaga et al., 2018; Carranza & Gille, 2015; Johnson, Plant, Dunne et al., 2017), water mass formation (Abernathey et al., 2016; Naveira-Garabato et al., 2009; Ohshima et al., 2013; Sallée et al., 2010), mixing in the Antarctic Circumpolar Current (Ledwell et al., 2011; Naveira Garabato et al., 2004, 2016), the overturning circulation (Marshall & Speer, 2012; Speer et al., 2000; Talley, 2013), and sea ice processes including its seasonal cycle and the associated freshwater cycle (Abernathey et al., 2016; Haumann et al., 2016). Dynamics of the Southern Ocean have commonly been oversimplified, although the tremendous diversity and nonzonality in Southern Ocean dynamical regimes are beginning to be appreciated (e.g., Masich et al., 2015; Sallée et al., 2010; Tamsitt et al., 2017; Thompson & Naveira Garabato, 2014). Because of this diversity, any comprehensive observing system for the Southern Ocean must be distributed over the entire region.

The global *core* Argo program of profiling floats has completely transformed global to regional observations of the physical state of the ocean, thus far providing nearly two decades of observations of seasonal cycle evolution and climate phenomena and change (Riser et al., 2016; Roemmich et al., 2009). Ice avoidance software, in place for almost a decade (e.g., Klatt et al., 2007; Wong & Riser, 2011), is now allowing Argo to expand south of 60°S. Profiling floats in the Weddell Sea that are also acoustically tracked have provided the only sustained under-ice measurements (Fahrbach et al., 2011). A marriage between ice-capable core Argo and maturing biogeochemical (BGC) sensing that resolves seasonal cycles in oxygen, nutrients, and carbon (Johnson et al., 2017) now allows us to map, quantify, and understand the unique biogeochemical and physical processes and their seasonal cycles in the Southern Ocean, where there have been almost no prior in situ winter biogeochemical observations. SOCCOM floats are BGC Argo floats (Biogeochemical-Argo Planning Group, 2016), following the same protocols as core Argo floats (10-day profiling from surface to 2,000 m, parking depth 1,000 m), with added BGC sensors (Riser et al., 2018). SOCCOM data are already improving forward ocean and climate models through direct comparison and state estimates that combine data and models (Russell et al., 2018).

The minimum spatial sampling density of BGC Argo floats required to resolve key features of the air-sea carbon exchange in the Southern Ocean has been tested in Observing System Simulation Experiments (OSSEs), suggesting 150–200 floats south of 30°S (Kamenkovich et al., 2017; Majkut et al., 2014; Mazloff et al., 2018). At this sampling density, the BGC floats form an intentionally incoherent array. When fully implemented, these 200 floats will constitute one quarter of the core Argo array of 800 south of 30°S. The strong relationship between the more densely sampled physical fields (T/S) and the more sparsely sampled biogeochemical parameters (oxygen, nitrate, and pH) should yield well-mapped biogeochemical fields (Giglio et al., 2018; Liang et al., 2018). The empirical algorithms employed in SOCCOM to calculate all carbonate system terms from the SOCCOM-observed properties (e.g., Carter et al., 2018, 2016; Williams et al., 2016) are successful because of similarly strong relationships between biogeochemical parameters. State estimates, which incorporate diverse observations such as core Argo and satellite data, provide dynamically consistent interpolation of ocean budgets (Wunsch & Heimbach, 2007). Central to SOCCOM is development of the biogeochemical Southern Ocean State Estimate, providing the first closed BGC budgets in the Southern Ocean constrained by BGC observations (Rosso et al., 2017; Verdy & Mazloff, 2017).

The heart of the SOCCOM-observing strategy is to ensure that all distinct water mass and dynamical regimes are sampled by BGC Argo floats. This aspect is only indirectly addressed by the OSSEs, which may lead to a random deployment approach. For SOCCOM, given the lack of prior year-round BGC information in most regions of the Southern Ocean, it would be irresponsible to deploy without considering regional conditions. Of course, until the full array is in the water, it is not possible to fully test whether all *important* regimes are covered, especially for wintertime properties/cycles. Hence, we rely on extensive historical knowledge of the biogeochemistry associated with water masses and circulation that controls them, principally from ship-based, nonwinter hydrography such as in the World Ocean Circulation Experiment (WOCE) and its descendant, GO-SHIP (http://go-ship.org). Regional circulation and water mass boundaries are strongly affected by topography, which we therefore take into account. As the mean biogeochemical structures beneath the seasonally warmed and freshened surface layer result from winter forcing and advection, we have good prior information in most regions about where to observe even without winter observations.

In section 2 we briefly describe the elements of selecting SOCCOM float deployment locations. Section 3 is an overview of SOCCOM float deployments at time of publication, through mid-2018.

In sections 4 and 5, we focus on the strategy for one of our earliest deployments, between South Africa and Antarctica along the so-called *Good Hope* line, or *A12* in WOCE and GO-SHIP (Koltermann et al., 2011). These 12 SOCCOM floats were deployed on the Polarstern PS89 cruise in 2014–2015 (Boebel, 2015). This was one of our largest deployments and provides us with three annual cycles to assess our strategy. Although the SOCCOM array now exceeds 108 floats (of 126 deployed), many do not yet have even one full annual cycle, and many are still near their deployment locations. PS89 deployment choices were based on the water mass, air-sea flux, and circulation structure from historical hydrographic data and particle trajectory analysis using existing Argo floats and two models. We evaluate this one set of deployment choices by comparing its 3 years of float trajectories with the ensemble OSSE and Argo trajectories (section 5.2) and briefly describe the water mass/circulation regimes covered thus far by these 12 floats in comparison with our original expectations (section 5.3 and supporting information). Since planning for PS89 in 2014, SOCCOM deployment strategy has evolved to include the biogeochemical version of Southern Ocean State Estimate (SOSE; Verdy & Mazloff, 2017) and statistical approaches for predicting SOCCOM float trajectories (Wang et al., 2018, and additional work in progress).

2. Elements of the SOCCOM Float Deployment Strategy

All SOCCOM floats are BGC-Argo floats. SOCCOM uses two types of enhanced Argo floats: UW-modified Teledyne Webb *Apex* floats and Seabird *Navis* floats. Each includes core Argo sensors (temperature, conductivity, and pressure) and, to the greatest extent possible, all BGC sensors (oxygen, nitrate, pH, and optical sensors—either chlorophyll fluorescence and backscatter on Apex or these plus fluorescence by color dissolved material on Navis floats), and ice avoidance software to enable winter profiling. SOCCOM follows Argo protocols for core properties (temperature, salinity, and pressure), cycling (parking at 1,000 m, profiling every 10 days from 2,000 m to the sea surface; Riser et al., 2018; Roemmich et al., 2009), and data management. SOCCOM core and BGC data are posted through the public real-time and delayed mode Argo data stream (http://jcommops.org). SOCCOM BGC data are also made available publicly in near real-time on the SOCCOM website, which also includes derived BGC properties (http://soccom.princeton.edu).

The SOCCOM float array, covering the ocean south of 30°S, is expected to reach full implementation of between 180 and 200 floats by 2020; ideally, this will be sustained indefinitely, requiring about 40 floats per year thereafter. Emphasis has been on deploying in the large seasonal ice region where there have been few Argo floats and few biogeochemical (BGC) measurements (cf. Johnson, Plant, Coletti et al., 2017; Johnson, Plant, Dunne et al., 2017). Deployments must take place gradually over the years because it is not possible to build a large fleet of BGC floats quickly and because some of the newer technology has required phased testing and implementation. Furthermore, because the float array must be phased in over 6 years, we had to begin with regional deployments.

While core Argo floats can be deployed from any vessel, SOCCOM uses research ships with CTD/water sample profiling capability to at least 1,500-m depth. Each SOCCOM float deployment is coincident with a hydrographic profile, which is used for validation of the float calibrations. Because BGC sensors can drift during the multiyear float lifetime, SOCCOM's calibration and postdeployment adjustment methods (Johnson, Plant, Coletti et al., 2017) cannot rely on direct adjustment of the float using coincident shipboard profiles, as crossover matching stations long after deployment are extremely rare. SOCCOM's calibration and postdeployment adjustment approach, backed by shipboard measurements at every SOCCOM float deployment to evaluate the calibration approach statistically, ensures that global BGC Argo, for which research ship deployment might not always be possible, is a realistic goal. Each SOCCOM shipboard profile includes discrete sampling for oxygen, salinity, pH, total alkalinity, nitrate, fluorescence, backscatter, high performance liquid chromatography (HPLC), and particulate organic carbon (POC; see shipboard sampling manual: Talley et al., 2017). The calibrated float data from the first float profile are compared retroactively with the coincident shipboard data, evaluated over the entire ensemble of SOCCOM floats. This provides validation and quality control of the calibration methods for each of the sensors.

SOCCOM relies on the network of Southern Ocean research expeditions organized by many nations (Table 1) and on cooperation between SOCCOM scientists and those of many other institutes and nations. Research cruises that make most of these measurements are most cost-effective; SOCCOM adds measurements where necessary. About half of the cruises have taken advantage of the international GO-SHIP program (http://go-

ship.org), which provides comprehensive, highly accurate measurements of the full water column that match most of the SOCCOM BGC sensors. GO-SHIP measures heat, freshwater, carbon, oxygen, and nutrient distributions throughout the world ocean, crossing each ocean basin once every 5 to 10 years (Talley et al., 2016). GO-SHIP produces high-quality, quick-turnaround, publicly available data sets (http://cchdo.ucsd.edu) and ensures that the gradually shifting relationship between biogeochemical parameters, which is central to BGC float calibration, is well observed. The synergy between GO-SHIP and Argo has been demonstrated in documentation of the ocean's heat and freshwater changes (e.g., Purkey & Johnson, 2010, 2013; Rhein et al., 2013); future years with expanding BGC Argo will provide an expanded focus on ocean carbon, nitrate, oxygen, and chlorophyll/particulates budgets.

SOCCOM deployment strategy steps for a given year and each research cruise are as follows. Application and evaluation of these steps for the Polarstern PS89 deployments are described in sections 4 and 5.

1. Determine number of floats available for the year (30 to 40)
2. Obtain information about international research expeditions with CTD/rosette capability, including GO-SHIP cruises, routine transit cruises operated by many Southern Hemisphere entities, and individually funded projects
3. Prioritize ship opportunities based on
    a. quality and completeness of planned shipboard measurements to minimize SOCCOM shipboard resources
    b. location relative to multiple oceanographic regimes and lack of BGC float time series
4. Review information about physical and biogeochemical regimes and categorize them for each cruise, with the goal of at least one float in each distinct water mass regime
5. Carry out quasi-Lagrangian analyses using simple particle-tracking OSSEs and historical Argo trajectories, with the goal of at least one float in each distinct circulation regime. Multiyear sea ice is avoided to facilitate annual reporting from under-ice floats.

3. SOCCOM Float Deployments: 2014–2017

During the SOCCOM proposal phase, we identified potential deployment opportunities based on known hydrographic cruises during the proposed 6 years (Figure 1a), to demonstrate feasibility using cruises of opportunity rather than dedicated ship time. Cruises for each austral summer season are identified and selected about 1 year in advance, when most institutions and groups have complete research cruise plans. Once a cruise is identified, a deployment plan is coordinated with the chief scientist, based on their planned CTD stations. Floats have been deployed on five to seven cruises each year, on research cruises from six different countries, commencing in early 2014 with pre-SOCCOM deployments from GO-SHIP P16S in the Ross Sea and South Pacific (Table 1 and Figure 1b). About half of the cruises are GO-SHIP, and about two thirds of the floats have been deployed from these usually longer GO-SHIP cruises. Only two cruises thus far, on transits of opportunity, have been mostly SOCCOM-supported and planned. Therefore, deployment locations must be planned in advance based on as much prior information as possible and cannot be adjusted based on in situ sampling during given cruises; this will also be the case for large-scale expansion of biogeochemical float deployments going forward.

We have endeavored to deploy in all sectors of the Southern Ocean without concentrating floats in any one region. Covering gaps in the Indian and Atlantic sectors is a focus in the remaining years. Sustaining the SOCCOM float array beyond 6 years, as floats complete their lifetimes, will require additional resources, similar to the continuously replenished *core* Argo float array and, assuming funding sources for the floats, should be achievable as long as the international GO-SHIP program and routine national Southern Ocean ship-based programs continue into the future.

4. A12 (0°E) and Weddell Sea Deployment Strategy

Our deployment strategy, based on prior information about hydrographic, circulation, forcing, and sea ice conditions along the research vessel track, is illustrated using the 12 SOCCOM floats deployed from the Alfred Wegener Institut's (AWI) Polarstern Expedition PS89 (ANTXXX-2) in 2014–2015 from Cape Town, South Africa, to Neumayer Station in Antarctica and then obliquely across the Weddell Sea (Boebel, 2015;

Table 1
SOCCOM Float Deployment Cruises (http://soccom.princeton.edu/), as of 4 August 2018

#	Ship Chief scientist	Name Cruise number Expocode	Dates	Total SOCCOM floats: Navis subset in parentheses
1	RVIB NB Palmer (U.S.) Lynne Talley (UCSD/SIO)	GO-SHIP P16S NBP1403 320620140320	20 Mar 2014 to 5 May 2014	12
2	RV Polarstern (Germany) Olaf Boebel (AWI)	(GO-SHIP) A12 ANT-XXX/2 PS89 06AQ20141202	2 Dec 2014 to 1 Feb 2015	12 (4 Navis)
3	RV Investigator (Aus.) Thomas Trull (CSIRO)	SOTS IN2015_V01 09IN20150321	21 Mar 2015 to 30 Mar 2015	2
4	RVIB NB Palmer (U.S.) Sebastien Bigorre (WHOI)	OOI SO NBP1511 320620151206	6 Dec 2015 to 2 Jan 2016	3
5	RV James Clark Ross (U.K.) Yvonne Firing (BAS)	GO-SHIP SR1B JCR15003 74JC20151217	17 Dec 2015 to 9 Jan 2016	4
6	RV Investigator (Aus.) Michael Coffin (U.Tas.)	HEOBI IN2016_V01 09IN20160108	8 Jan 2016 to 5 Mar 2016	3
7	RVAurora Australis (Aus.) Andrew Constable (AAD)	K-Axis Voyage V3 09AR20160111	11 Jan 2016 to 25 Mar 2016	2 (2 Navis)
8	RV Roger Revelle (U.S.) Alison Macdonald (WHOI)	GO-SHIP I8S RR1603 33RR20160208	8 Feb 2016 to 21 Mar 2016	6 (2 Navis)
9	RV Investigator (Aus.) Peter Strutton (CSIRO)	Eddy IN2016_V02 09IN20160314	14 Mar 2016 to 13 Apr 2016	2
10	RV Investigator (Aus.) Bernadette Sloyan (CSIRO)	GO-SHIP P15S IN2016_V03 09IN20160426	27 Apr 2016 to 27 May 2016	13 (5 Navis)
11	RV Ron Brown (U.S.) Rolf Sonnerup (NOAA)	GO-SHIP P18 RB-16-06 33RO20161119	28 Dec 2016 to 3 Feb 2017	7
12	Akademik Tryoshnikov (RU) David Walton (BAS)	ACE Leg 1 RUB320161220	20 Dec 2016 to 19 Jan 2017	4 (2 Navis)
13	RVIB NB Palmer (U.S.) Stephen Riser (UW)	HazMat NBP1701 320620161224	24 Dec 2016 to 20 Jan 2017	12 (2 Navis)
14	RV Mirai (Japan) Hiroshi Uchida (JAMSTEC)	GO-SHIP P17S MR16–09 49NZ20170208	8 Feb 2017 to 5 Mar 2017	5
15	RVIB NB Palmer (U.S.) Stephen Ackley (UTexasA)	PIPERS NBP1704 320620170410	10 April 2017 to 14 June 2017	4
16	RVIB NB Palmer (U.S.) Sabine Mecking (UW) and Kevin Speer (FSU)	GO-SHIP P6 NBP1706 320620170703	3 July 2017 to 30 Sept 2017	6
17	SA Agulhas II (South Africa) Tahlia Henry (U. Cape Town)	Gough transit AGU027 91AH20170907	7 Sept 2017 to 12 Oct 2017	6
18	SA Agulhas I (South Africa) Anil Kumar (NCAOR, Goa, India)	NCAOR SOE2017–18	9 Dec 2017 to 4 Feb 2018	7 (2 Navis)
19	RV Investigator (Aus.) Steve Rintoul (CSIRO)	GO-SHIP SR3	10 Jan 2017 to 22 Feb 2018	11 (1 Navis)
20	RVIB NB Palmer (U.S.) Alison Macdonald (WHOI)	GO-SHIP S04P	9 March 2018 to 13 May 2018	6
	8 countries 12 non-U.S. cruises 8 U.S. cruises	10 GO-SHIP 10 non GO-SHIP		78 GO-SHIP 49 non GO-SHIP

Note. The expocode is the identifier for the shipboard data sets assembled after each cruise and archived at the Carbon and Climate Hydrographic Data Office (CCHDO; http://cchdo.ucsd.edu).

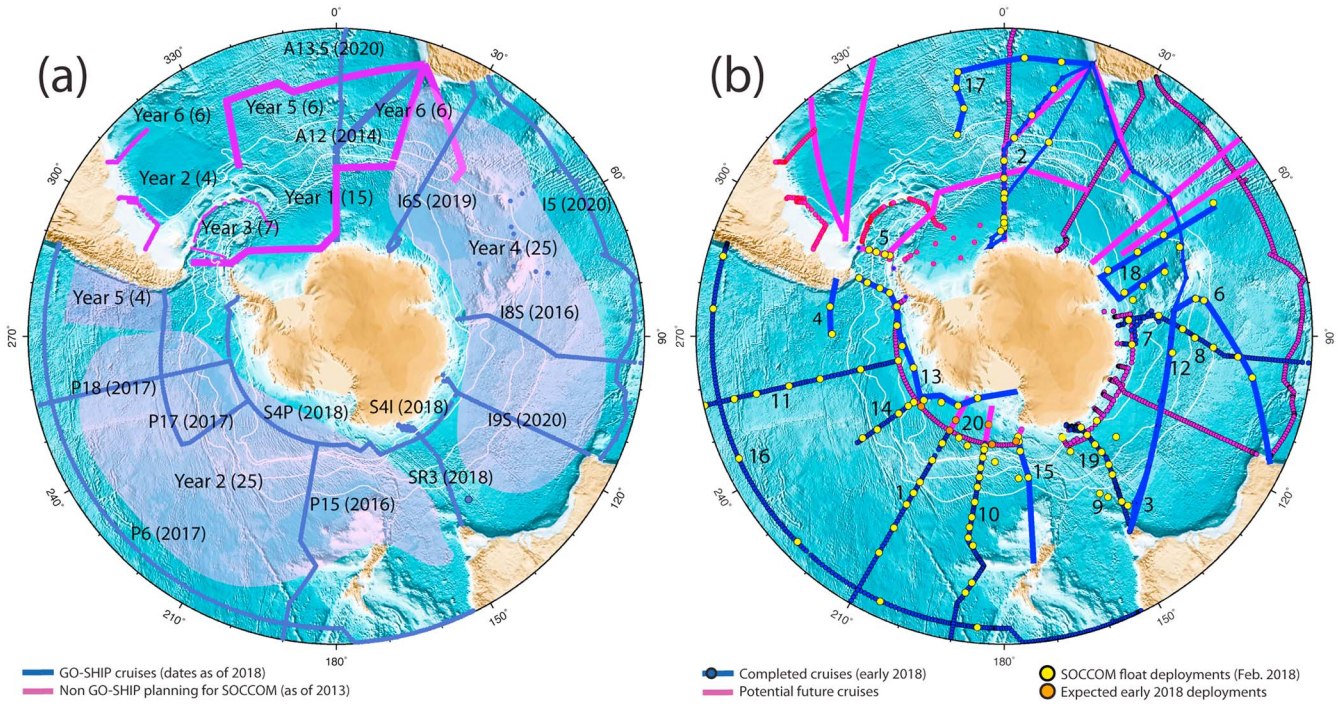
(a)
A13.5 (2020)
Year 6 (6)
Year 5 (6)
Year 6 (6)
A12 (2014)
Year 2 (4)
Year 1 (15)
I6S (2019)
I5 (2020)
Year 3 (7)
Year 4 (25)
Year 5 (4)
I8S (2016)
P18 (2017)
P17 (2017)
S4P (2018)
S4I (2018)
I9S (2020)
Year 2 (25)
SR3 (2018)
P15 (2016)
P6 (2017)
GO-SHIP cruises (dates as of 2018)
Non GO-SHIP planning for SOCCOM (as of 2013)
(b)
Completed cruises (early 2018)
Potential future cruises
SOCCOM float deployments (Feb. 2018)
Expected early 2018 deployments

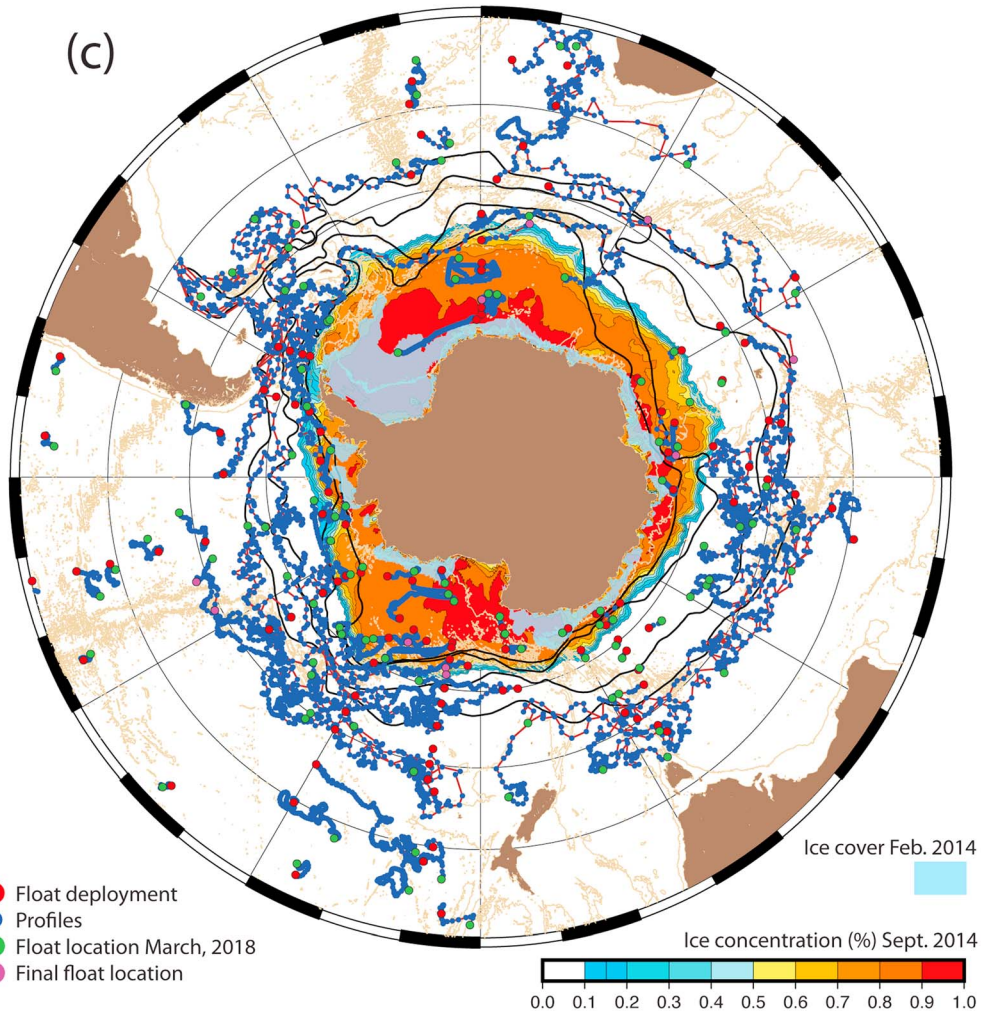
(c)
Float deployment
Profiles
Float location March, 2018
Final float location
Ice cover Feb. 2014
Ice concentration (%) Sept. 2014
0.0 0.1 0.2 0.3 0.4 0.5 0.6 0.7 0.8 0.9 1.0

Figure 2). The biannual AWI expeditions along this *Good Hope line* include hydrographic stations along WOCE/GO-SHIP sections A12 and A23 (Fahrbach et al., 2011; Koltermann et al., 2011), servicing of moorings, and biological measurements (Boebel, 2015).

In the north, this transect crosses the energetic eddy field in the Cape Basin near Africa, which arises from Agulhas retroflection and ring shedding (e.g., Richardson, 2007; Figure 3). The transect then crosses the Antarctic Circumpolar Current, which flows eastward from the Atlantic to the Indian Ocean. In the south, A12 crosses the cyclonic Weddell Gyre.

PS89 was the first formal SOCCOM deployment cruise, the first set of SOCCOM floats in the Atlantic and Weddell Sea, and the first internationally coordinated SOCCOM float deployment. The planned and actual PS89 stations and SOCCOM float deployments are shown in Figure 2 (Boebel, 2015; Knust, 2014; Talley et al., 2015). The planned Weddell Sea crossing was canceled during the cruise (section 5.1), so floats designated for that region were deployed on the return transit to South Africa, hence also near A12.

Many background materials are used together to select deployment locations, presented here in three sections: topography, climatological circulation, fronts and frontal zones, sea ice, and surface forcing (section 4.1); water mass analysis relative to fronts and circulation (section 4.2); and prior float and simulated float trajectories (section 4.3). Our final deployment choices are described in section 4.4.

4.1. Regional Overview: Climatological Setting, Surface Properties, and Fluxes

Hydrographic/biogeochemical properties along the A12 Good Hope section (section 4.2) and circulation analysis (section 4.3) were the principal tools for deployment selection. But for every cruise, we start by characterizing the large-scale, climatological setting. Mean circulation and mesoscale variability, fronts and frontal zones, topography, sea ice, winds, surface fluxes of buoyancy, heat and carbon, mixed layer depth, and biomes (biological regimes) are each essential for choosing float locations. They remain essential for understanding the properties, observed surface fluxes, and trajectories of the floats over the several years since deployment (section 5). Our own growing biogeochemical float data set has increasingly become part of this evaluation but of course was unavailable for PS89 (e.g., Arteaga et al., 2018; Briggs et al., 2018; Gray et al., 2018; Johnson, Plant, Dunne et al., 2017; Williams et al., 2017).

4.1.1. Mean Circulation, Fronts, Frontal Zones, and Mesoscale Variability

There are three overall *mean circulation* regions along the A12 section, which also map onto the three largest classes of water mass regimes. Multiple PS89 SOCCOM floats were deployed in each regime. These are (i) the subtropical/subantarctic region north of the Antarctic Circumpolar Current (ACC), (ii) the ACC, and (iii) the Weddell Gyre sea ice zone south of the ACC (Table 2). These three are separated by the northernmost and southernmost ACC fronts: the Subantarctic Front (SAF) and Southern Boundary (SBDY). The mean circulation at 1,000-m depth (float parking depth) is similar to the surface circulation, which is depicted schematically (Figure 3a) and from satellite altimetry (Figure 3b; e.g., Fahrbach et al., 2011; Orsi et al., 1993, 1995; Reid, 1994, 2003; Talley et al., 2011). This equivalent barotropic structure is typical of high-latitude oceans. Along A12 it is absent only in the northernmost subtropical Cape Basin region, where deep waters flow southward beneath the northward Benguela, joining the eastward flow of North Atlantic Deep Water (NADW) crossing the South Atlantic (Garzoli et al., 2015; Reid, 1994; Tamsitt et al., 2017; Tsuchiya et al., 1994; van Sebille et al., 2012). This eastward boundary flow is largely below 2,000 m, and so Argo float trajectories are mostly unaffected by it, although the deepest properties sampled by the floats are within this deep water layer.

Each of the three major circulation regimes has important subdivisions that are marked by fronts (Table 2 and Figure 3), as follows. Note that while frontal locations/velocity structure can be synoptically complex (e.g., Sokolov & Rintoul, 2009), the frontal zones between the fronts characterize the water mass regimes well.

(i) The subtropical circulation between Africa and the SAF includes northwestward flow into the Benguela Current, eastward flow in the Subtropical Front (STF), and eastward flow of the subtropical gyre north

Figure 1. SOCCOM float deployment planning and current status. (a) Deployment cruises for 2014–2020 as proposed in 2013, including international GO-SHIP sections (http://goship.org; blue), and expected non GO-SHIP cruises (magenta), with proposed number of floats; these opportunities have evolved significantly. (b) Current status of deployments (Table 1): March 2014 to March 2018. (c) Profile locations through February 2018, with trajectories, representative September sea ice concentration (%) and February sea ice extent from the National Snow and Ice Data Center (Maslanik & Stroeve, 1999, updated daily), and 3,000-m isobath (light brown) from etopo2 (Smith & Sandwell, 1997). Antarctic Circumpolar Current front representations (white in a and b and black in c) from Orsi et al. (1995).

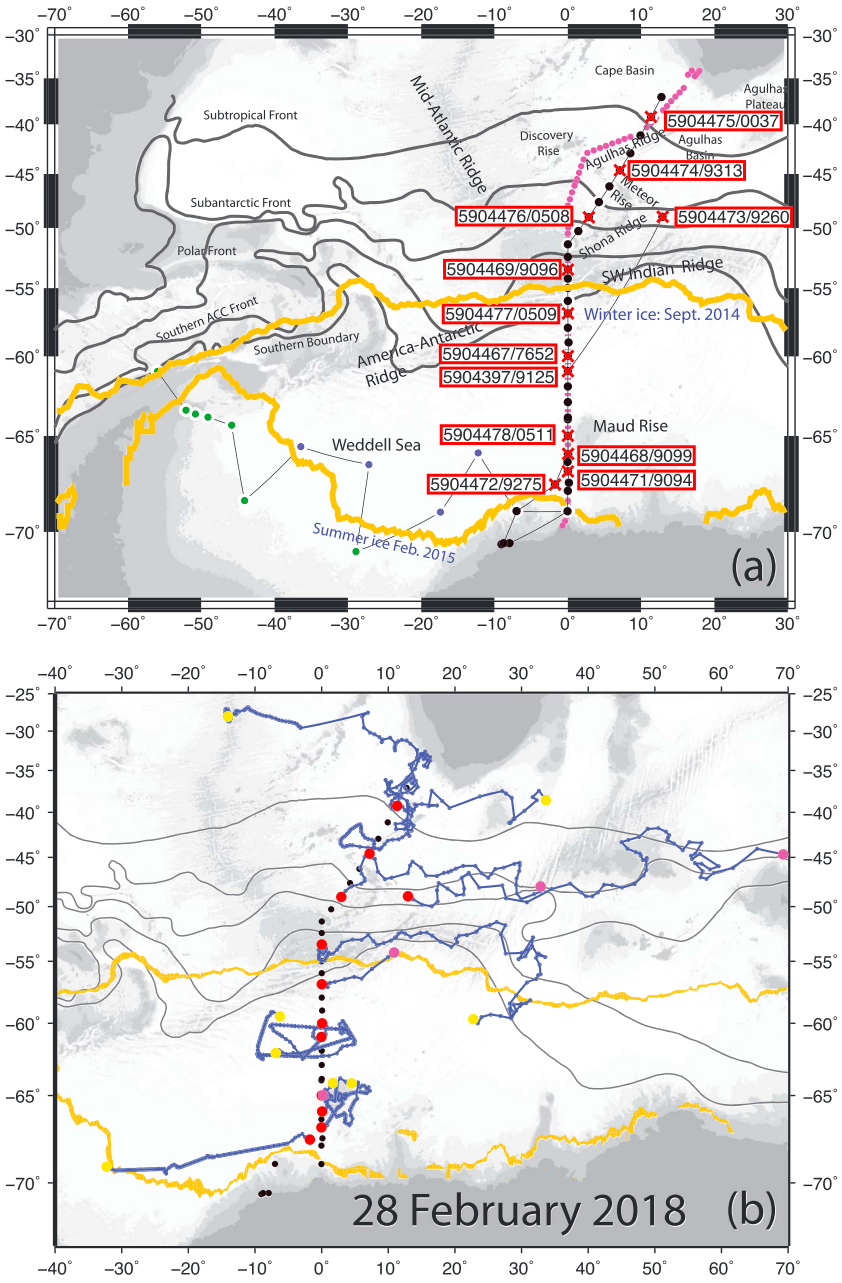

Figure 2. RV Polarstern PS89 (ANT-XXX/2, 2 December 2014 to 1 February 2015). (a) Planned stations and actual deployments. Red crosses and boxed labels: SOCCOM float deployments, labeled with WMO ID/U. Washington ID (see http://soccom.ucsd.edu/floats/SOCCOM_data_ref.html; Talley et al., 2015). Black dots: PS89 stations (Boebel, 2015). Blue/green dots with white circles: PS89 planned floats/stations prior to cruise (Knust, 2014). Magenta dots: WOCE section A12 (Polarstern ANT-X/4, 21 May 1992 to 5 August 1992, https://cchdo.ucsd.edu/cruise/06AQANTX_4). (b) Trajectories for SOCCOM floats through May 2017: red (start), yellow (May 2017), magenta (last profile). Black dots: PS89 stations. In both figures, orange bands are 10–20% sea ice concentration in September 2014 (winter, precruise) and February 2015 (summer, postcruise), black curves are representative front locations based on historical hydrographic data (Orsi et al., 1995) and topography is etopo2 (Smith & Sandwell, 1997).

and south of the STF. East of A12, but potentially accessible to floats deployed from A12, is the eastward Agulhas Return Current (section 4.2). The frontal zones in this region are the Subtropical and Subantarctic Zones (STZ and SAZ), separated by the STF. SOCCOM floats should be deployed in both the STZ and SAZ.

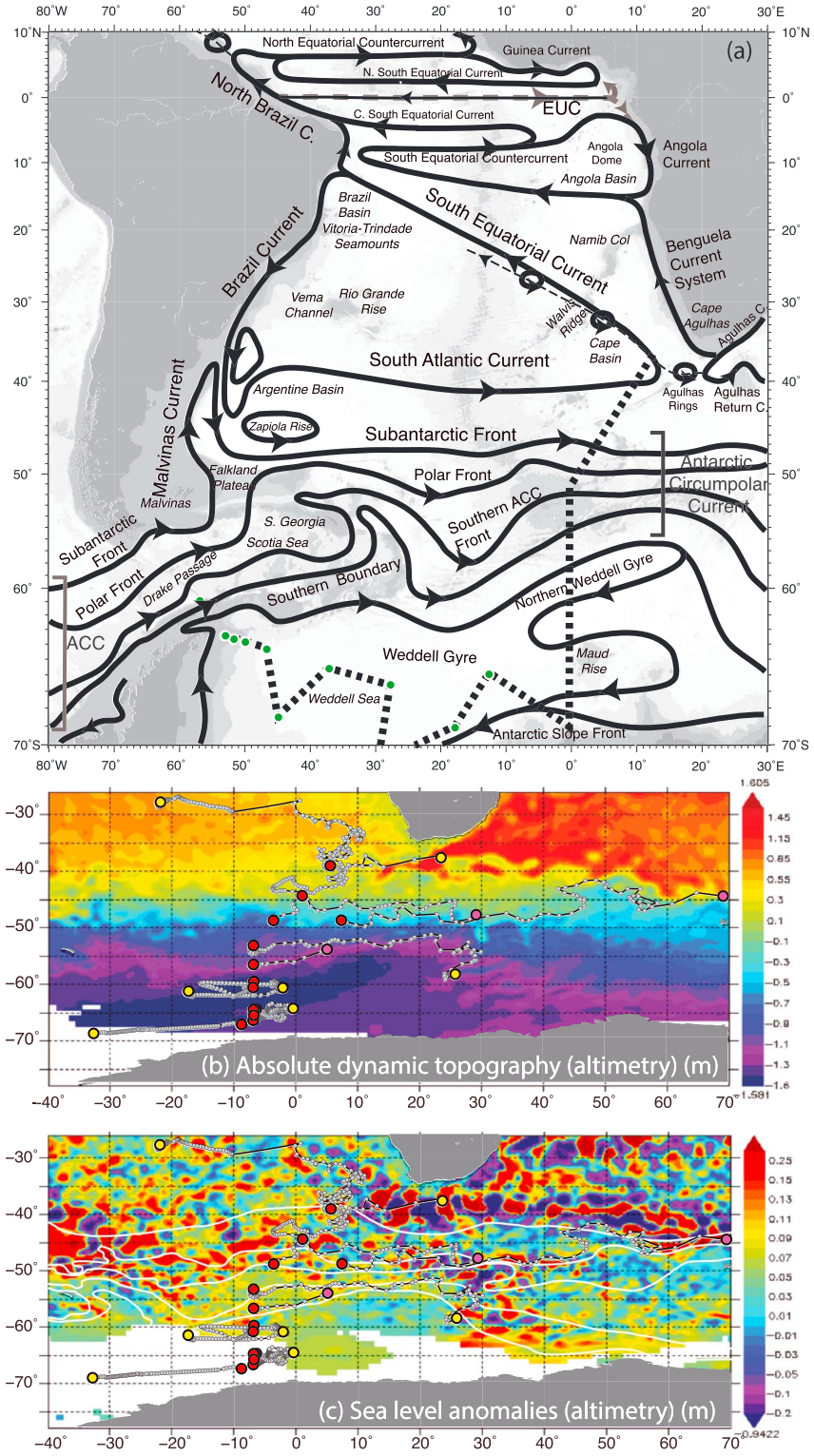

Figure 3. (a) Schematic surface circulation of the South Atlantic, modified from Talley et al. (2011), with planned RV Polarstern PS89 (ANTXXX-2) track superimposed (dashed and green dots in Weddell Sea). Weddell Sea modifications are from Orsi et al. (1993); Zapiola Rise circulation in Talley et al. has been corrected. (b) Absolute dynamic topography (m) and (c) sea surface height anomalies (m), both from Aviso satellite altimetry on 1 December 2014 (http://las.aviso.altimetry.fr/las/getUI.do), with SOCCOM float tracks as of 28 February 2018 (red: deployment; yellow: current position; magenta: final position), and historical front locations from Orsi et al. (1995; white) (from south to north: SBDY, SACCF, PF, SAF, STF).

Table 2
Circulation and Water Mass Regimes (Fronts and Frontal Zones) Along the Good Hope Section (A12; Orsi et al., 1995; Talley et al., 2011), With Number of SOCCOM Floats That Were Planned/Deployed

Regime	Boundaries on A12 (north and south) (Figure 5)	Expected flow direction	Water properties on A12 (Figure 5)	# floats planned/ deployed	WMO ID/UW ID N (avis) or A (pex)	# profiles as of 5 August 2018
1. Subtropical Zone (STZ) (Subtropical gyre and Cape Basin)	African coast and Subtropical Front (STF)	Northwestward gyre flow, Benguela Current, Agulhas rings	Warm (>15 °C), saline (>34.6) surface waters; weak AAIW salinity minimum; core NADW	1/1	5904475/0037 N	143
2. Subantarctic Zone (SAZ)	Subtropical Front and Subantarctic Front (SAF)	Eastward	Warm (8–9 °C), high-oxygen upper layer; strong AAIW salinity minimum/oxygen maximum	1/1	5904474/9313 A	148
3. ACC Polar Frontal Zone (PFZ)	Subantarctic Front and Polar Front (PF)	Eastward	Lower salinity surface water, monotonically decreasing temperature with depth, high oxygen	1/2	5904476/0508 N 5904473/9260 A	55 (D) 67 (D)
4. ACC Antarctic Zone (AZ)	Polar Front and Southern ACC Front (SACCF)	Eastward	Freshest surface water, temperature minimum and maximum structure, strongly southward shoaling O_2 min reaching almost 200 m	0/0	(none)	
5. ACC Southern Zone (SoZ)	SACCF and ACC Southern Boundary (SBDY)	Eastward	Lowest salinity surface water, cold surface water, temperature maximum, shoaled deep water properties including low oxygen	2/2	5904469/9096 A 5904477/0509 N (also Northern Weddell Gyre)	130 20 (D)
6. Northern Weddell Gyre (NWG)	ACC Southern Boundary and Maud Rise	Cyclonic gyre	Sea ice, temperature and salinity minimum at surface in winter, temperature maximum and oxygen maximum subsurface	1/2	5904467/7652 A 5904397/9125 A	129 (UI) 114
7. Maud Rise (0°E) (Weddell Gyre)	Maud Rise and Antarctic Slope Front (ASF)	Cyclonic gyre (local)	Sea ice, as above	1/3	5904478/0511 N 5904468/9099 A 5904471/9094 A	4 (D) 122 (UI) 125 (UI)
8. Continental Zone (Weddell Gyre)	Antarctic Slope Front and Antarctic coast	Westward (high speed)	Sea ice, as above	1/1	5904472/9275 A	115 (UI)
9. Weddell Sea (Weddell Gyre)	Weddell Sea west of 10°W	Cyclonic gyre	Sea ice, as above	4/0	(none)	-

Note. Heavy lines separate the subtropical, ACC, and Weddell regions. Number of profiles includes status (D) if the float is no longer operating and (UI) if float is under ice as of 5 August 2018. The four planned Weddell Sea floats were deployed on the return transit to Cape Town after ship malfunction. Supporting information Table S1 includes additional information about the deployed floats.

(ii) The overall eastward flow of the ACC includes several permanent, circumpolar fronts—the SAF, Polar Front (PF), Southern ACC Front (SACCF), and SBDY. The zones within the ACC between these fronts are the Polar Frontal, Antarctic, and Southern Zones (PFZ, AZ, and SoZ; Orsi et al., 1995; Kim & Orsi, 2013). SOCCOM floats should be deployed in each of three frontal zones.

(iii) The overall cyclonic circulation of the Weddell Gyre, which is ice covered in winter (section 4.1.2), includes a northern Weddell Gyre, an anticyclonic deviation north of Maud Rise, and westward flow along the Antarctic continental slope (Fahrbach et al., 2011). Maud Rise is important for polynya formation (Gordon, 1978; Swart et al., 2018), its tendency to trap floats in a Taylor column (Bersch et al., 1992; Klatt et al., 2007; Muench et al., 2001; Ou, 1991), and its unusual ecosystem (Brandt et al., 2011). At least one SOCCOM float should be deployed in each of these three Weddell subregions.

Mesoscale variability is also important for identifying oceanographic regimes, affecting mixing of water properties and float dispersion within the mean flow (e.g., Davis, 1991; LaCasce, 2008). Mesoscale variability in the A12 region, represented here by altimetric sea surface height anomalies (Figure 3c), aligns with the mean circulation regimes. The most energetic eddy field is in the north, associated with the Agulhas retroflection and Cape Basin (Ducet et al., 2000; Lumpkin & Johnson, 2013; Richardson, 2007). Float dispersion can be expected to be strong here. In addition, floats caught in Agulhas rings could be advected northwestward with the rings, although we note that profiling, hence quasi-Lagrangian, floats do not usually remain trapped in eddies due

to vertical shear within the eddy (e.g., Riser, 1982). The eddy field drops off south of about 40°S (at the STF) and remains at a medium level in the SAZ and within the ACC even though this is the region of highest mean kinetic energy (strongest currents). EKE is lowest in the Weddell gyre. These eddy energy features are apparent in Davis (2005). To the east of A12, near 30°S, 50°E, in a region that was crossed by PS89 floats after deployment, there is a major hot spot of EKE where the ACC fronts cross the Southwest Indian Ridge (e.g., Ducet et al., 2000; Tamsitt et al., 2017; Thompson & Sallée, 2012). In a complementary view, eastward moving coherent eddies are concentrated within the ACC along about 50°S (Chelton et al., 2011), even though this region has relatively low EKE. SOCCOM floats deployed in each of the mean circulation regimes and frontal zones will capture the main features of the EKE field.

Based on just this circulation and frontal analysis, we tentatively identified the nine distinct regimes listed in Table 2. These choices will be discussed in later sections in terms of geography, surface forcing, water masses, and detailed circulation projections. With only 12 floats to deploy from PS89, we attempted at least one in each of the nine regimes. These are the coarsest subdivision that provides coverage of all water masses and mean circulation structures, especially those relevant to air-sea carbon flux.

4.1.2. Topography and Sea Ice

Topography and seasonal sea ice (Figure 2) provide geographic context. Many fronts along A12 are associated with topography (Figure 5 in section 4.2), hence have predictable locations. The winter sea ice edge is associated with the ACC SBDY, which follows an undersea ridge across A12.

PS89 angled southwest from Cape Town across the Cape Basin, crossing several ridges and a small corner of the Agulhas Basin, to the triple junction of the Mid-Atlantic Ridge, America-Antarctic Ridge, and Southwest Indian Ridge. (The A12 section in 1992 [Figure 2a and section 4.2] crossed to Discovery Rise, staying completely within the Cape Basin until reaching the triple junction.) From there, the track was southward along the Greenwich meridian across the Weddell Sea to the Antarctic coast. The track passed west of Maud Rise, where a large polynya occurred in the late 1970s (Gordon, 1978; Gordon et al., 2007; Martinson et al., 1981; Muench et al., 2001; Weijer et al., 2017). An unexpected recurrence of the Maud Rise polynya in 2016 and 2017 (Swart et al., 2018) was captured by two PS89 SOCCOM floats (5904471 and 5904468). The SACCF and SBDY are tied to underlying ridges and bracket the location of deep water upwelling in the ACC Southern Zone (section 4.2), which has now been shown from SOCCOM floats, including PS89 float 5904469 (Figure 2a), to be a major axis of ocean carbon outgassing (Gray et al., 2018).

SOCCOM seeks to increase the number of Argo floats in the seasonal sea ice zone, where sea ice detection software protects the floats from surfacing under ice, with all under-ice profiles reported when the float surfaces in ice-free conditions (Chamberlain et al., 2018; Klatt et al., 2007; Wong & Riser, 2011). We used summer ice edges, the mean circulation, previous Argo trajectories, and float trajectories simulated in numerical models (section 4.3 below) to select float deployment locations likely to produce at least one annual cycle before entering multiyear ice. Thus, we excluded deployment locations at the southernmost and northwesternmost stations in the Weddell Sea, within the summer ice limit shown in Figures 1c and 2. Seven of the 12 PS89 floats were deployed in the seasonal ice zone, and none have entered the multiyear pack as of mid-2018, although one (ASF 5904472) is approaching it in its fourth year.

4.1.3. Climatological Surface Forcing

While the basic description provided thus far has served to define the important oceanographic regimes, these regimes are created by or characterized by particular surface forcings (Figure 4), including winds, heat/freshwater/buoyancy fluxes, and carbon fluxes. Analysis of the float observations is carried out in the context of these forcings.

4.1.3.1. Wind Stress and Wind Stress Curl (Figure 4b)

Winds are westerlies between Africa and about 65°S, with a maximum near 50°S, and easterlies from 65°S to the continent, increasing in strength to the coast. This results in Ekman downwelling north of 50°S and upwelling to the south. Within the subtropics, near Africa, there is enhanced downwelling offshore of the eastern boundary Benguela Current upwelling region. Downwelling persists southward across the SAF and ends at the historical PF location. Upwelling increases southward from there through the AZ, SoZ, and through the Weddell Gyre, reaching a maximum within a narrow offshore band due to the strong coastal easterlies. These drive downwelling along the coast (not represented in Figure 4). Floats planned for north (south) of the PF are therefore in downwelling (upwelling) zones, with extremes offshore of the Benguela region (Antarctic coastline region).

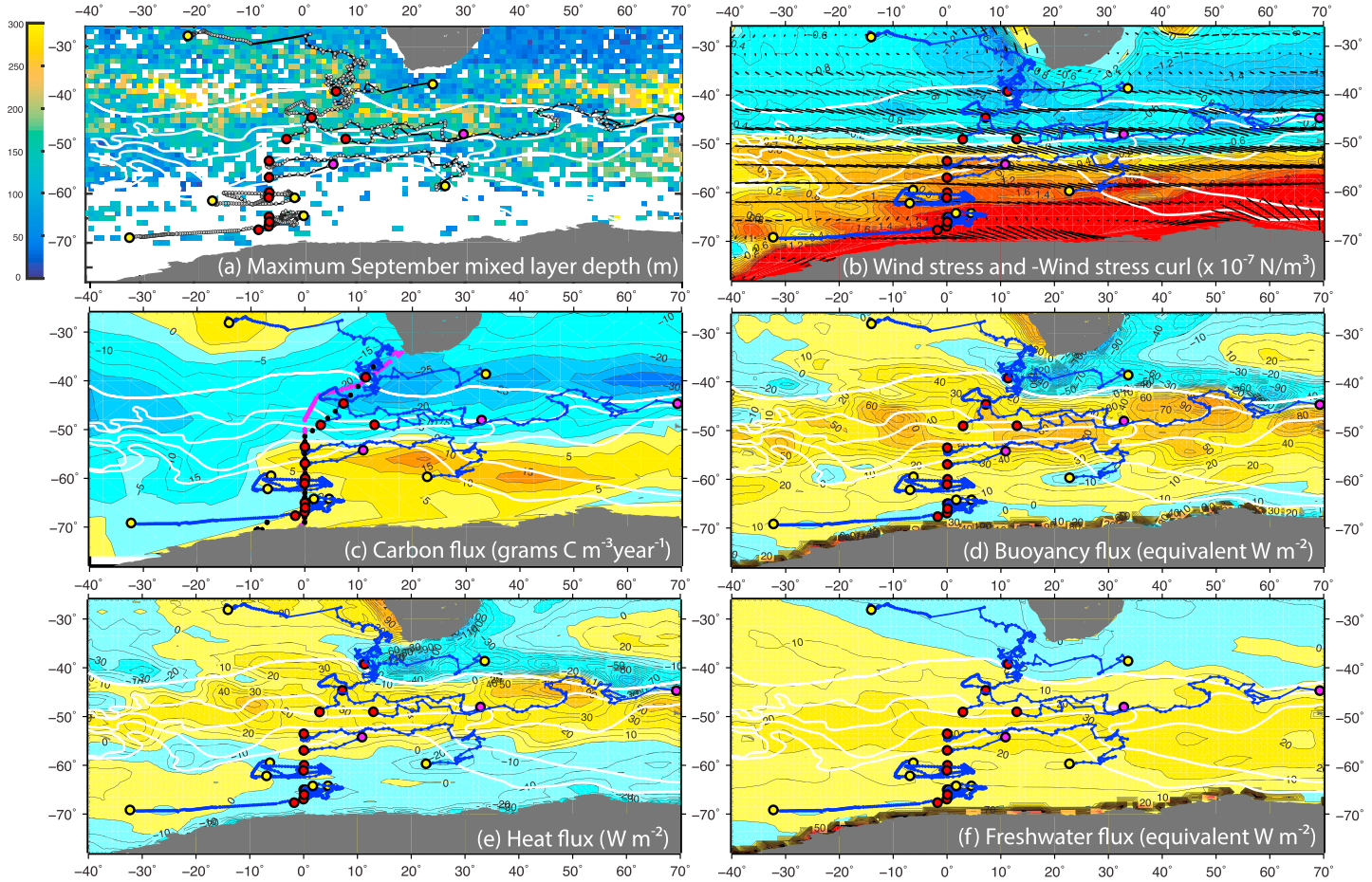

Figure 4. (a) Average maximum September mixed layer depth (m) from all Argo profiles 2000–2016, using density threshold criterion, in each 1° latitude/longitude bin (Holte et al., 2017; http://mixedlayer.ucsd.edu). White bins have no September profiles. (b) Wind stress (vectors; N/m^2) and negative wind stress curl (× 10^{-7} N/m^3) from NCEP reanalysis 1968–1996 (Kalnay et al., 1996). (c) Surface carbon flux (grams C/m^{2}yr) (Takahashi et al., 2009). Positive is flux out of the ocean (outgassing). (d) Annual mean surface buoyancy flux converted to equivalent heat flux (W/m^2), summed from (e) annual mean surface heat flux and (f) annual mean freshwater flux converted to equivalent heat flux, all from Large and Yeager (2009), following Cerovecki et al. (2011). Positive values are flux into the ocean, reducing density. In all panels: RV Polarstern PS89 float deployment locations (red), location at end of February 2018 (yellow), or final location (large magenta). Climatological frontal locations (white) from Orsi et al. (1995) (from south to north: SBDY, SACCF, PF, SAF, STF).

4.1.3.2. Air-Sea Fluxes of Heat, Freshwater, and Buoyancy (Figures 4d–4f)

Buoyancy flux, in equivalent heat flux units, is positive in most of this region; that is, surface water becomes less dense despite these high latitudes (e.g., Cerovecki et al., 2011). The highest positive buoyancy inputs are in the Benguela Current and along the ACC axis. The Benguela is a classic upwelling system in which cool upwelled water is warmed. The high buoyancy input in the ACC is due to warming of the northward Ekman flux of cool water (Tamsitt et al., 2016) and net precipitation (Figure 4f); the freshwater input is greater than shown because of sea ice melt at the outer edge of the seasonal ice region (Abernathey et al., 2016). This ACC buoyancy input creates the classic upper limb of the Southern Ocean overturning circulation, in which upwelled ACC waters moving northward through Ekman transport become lighter and subduct due to Ekman downwelling and encounter with less dense surface waters to the north.

The greatest buoyancy loss is in the north, in the Agulhas and Agulhas Return Currents. This is the largest net heat loss region of the Southern Hemisphere, rivaling that of the major Northern Hemisphere subtropical boundary currents, the Gulf Stream, and Kuroshio. Heat loss here is due to southward advection of warm waters in the western boundary current, encountering cool air (Tamsitt et al., 2016). Heat loss extends into the South Atlantic following the path of warm Agulhas waters, which is also a region of net evaporation and Ekman downwelling.

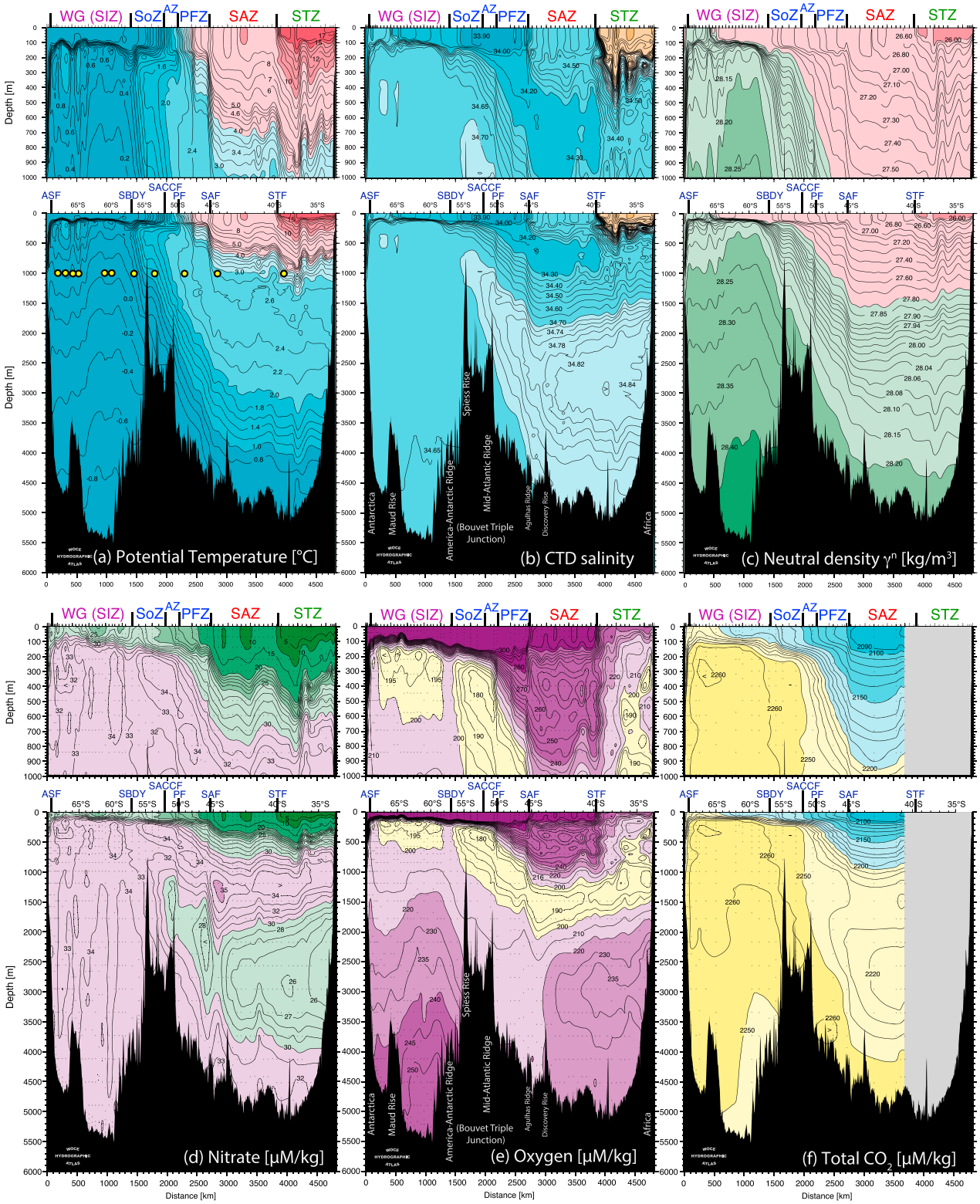

Figure 5. Vertical sections along World Ocean Circulation Experiment (WOCE) Hydrographic Programme (WHP) section A12 from the WHP Atlantic Atlas (Koltermann et al., 2011), annotated with topographic and frontal features: (a) potential temperature (°C), (b) salinity, (c) neutral density (kg/m^3), (d) nitrate (μmol/kg), (e) oxygen (μmol/kg), and (f) dissolved inorganic carbon (μmol/kg). WHP section A12 was occupied 21 May 1992 to 5 August 1992. Station positions are shown in Figure 2a. The 2014–2015 PS89 section followed a similar track, with differences at the northern end. SOCCOM float latitudes are shown in panel (a), at 1,000 m, which is the float parking depth.

South of the ACC in the seasonal sea ice zone of the eastern Weddell Sea, net buoyancy input is nearly neutral, a balance of net cooling and net freshwater input. Brine rejection due to sea ice formation and freshwater input due to sea ice melt are not captured in these maps but produce result in net freshwater flux where they are separated spatially, with net salinification at the Antarctic coastline and north of Maud Rise and net freshening at the northern sea ice edge (e.g., Abernathey et al., 2016).

Floats placed relative to these fluxes should include the net buoyancy gain and loss regions (ACC and Agulhas) and divisions of the sea ice zone in the Weddell Gyre: north of Maud Rise where there is moderate upwelling and buoyancy input, the Maud Rise region where sea ice is weak due to upward mixing of subsurface heat (Bersch et al., 1992; de Steur et al., 2007), and the continental boundary region of strong upwelling and sea ice formation.

4.1.3.3. Air-Sea Carbon Flux

Knowledge of annual mean carbon fluxes for cruise planning was based on Takahashi et al. (2009), which has very coarse resolution of 5° × 4° (Figure 4c) and little winter data. This coarse-resolution product shows ocean carbon uptake north of 55°S, which is roughly the ACC PF or SBDY, and roughly coinciding with the zero of Ekman pumping (Figure 4b). Greatest uptake is around 45°S where surface cooling is maximum (Figure 4e). Maximum outgassing is around 57°S at the ACC SBDY, where waters are warming but where there is also a subsurface source of upwelled carbon. The Weddell Gyre outgasses west of the A12 section, in the heavy sea ice region, and takes up carbon to the east, roughly coinciding with surface cooling and heating, respectively. Our subsequent float results are beginning to sharpen this regional flux description (Gray et al., 2018; section 5.3 below). The SOCAT neural network-based carbon flux product (Landschützer et al., 2014) was not used for PS89 but is incorporated in our more recent planning.

4.1.4. Climatological Winter Mixed Layers and Biogeography

The *surface mixed layer* strongly impacts biogeochemistry. Deep winter mixed layers north of the SAF are the source of the weakly stratified Subantarctic Mode Water (SAMW; Hanawa & Talley, 2001; McCartney, 1982; Figure 4a). The Atlantic form of SAMW is present on the A12 section in the SAZ between 45°S and the Subtropical Front, where winter mixed layer depths are between 250 and 300 m (Figures 4a and 5c; Holte et al., 2017); this SAMW is much weaker than in the eastern Indian and Pacific Oceans but nonetheless is an important regional signal. Along A12, southwest of Africa, SAMW coincides with high anthropogenic carbon (ACO_2) inventory (Khatiwala et al., 2013). Even higher ACO_2 is found southeast of Africa, associated with Agulhas Return Current (ARC) processes rather than with the SAMW south of the ARC. Deployment of BGC floats in these deep SAMW mixed layers and high ACO_2 inventory regions is essential for tracking the Southern Ocean's role in the carbon budget. Deployment in the deep mixed layer region of the SAZ is thus a priority.

Surface chlorophyll and particulate inorganic carbon satellite products (Balch et al., 2011; Moore & Abbott, 2000; Talley et al., 2011, Figures 4.28 and 4.29) were consulted for SOCCOM's fluorescence and backscatter sensors. Backscatter responds to both particulate inorganic carbon (PIC) and POC. Ocean color and PIC have a nearly zonal boundary at about 30° to 35°S in the Atlantic and Indian Oceans, oligotrophic to the north and productive to the south. This is governed by near-surface nitrate availability and is closely aligned with the zero zonal wind stress (Figure 4b), which is the northern boundary of equatorward Ekman transport of nutrient-rich, upwelled water. PIC is high in a zonal band (*Calcite Belt*) between 35°S and the Subantarctic Front in this region, decreases within the ACC, and then increases southward to a maximum in the Weddell Gyre and continental region, aligned there with high upwelling (Balch et al., 2011). Also in the A12 region, the Benguela upwelling regime has high chlorophyll in all seasons; in austral winter months, higher concentrations of chlorophyll fan out westward into the subtropical South Atlantic. Placement of SOCCOM floats across the 35°S productivity horizon and the STF, and within the broad Benguela region, was thus important for delineating productivity regimes. High PIC along the Agulhas Return Current and near the Antarctic coast should also be sampled by SOCCOM floats.

After planning was completed for PS89, several major publications delineating the overall biogeography of the Southern Ocean, including this region, were published (Ardyna et al., 2017; Fay & McKinley, 2014) and are useful for current SOCCOM float deployment planning. The boundaries of biological regimes likely have controls in addition to the physical forcings that delineate heat, salt, oxygen, DIC, and nutrient regimes. Moving forward with BGC-Argo, all of these controls and regimes will be taken into account.

4.2. A12 Water Mass Structure

In section 4.1 we used climatological analyses to define three overarching regions and nine subregions to be seeded with SOCCOM floats. Here we look at the detailed structure of the water masses and frontal structures along the section, to form a much better idea of what we expect to see from floats deployed in these regions and to refine the deployment strategy if needed. For deployment cruises along routinely sampled BGC hydrographic sections, such as this A12 section and any GO-SHIP lines, water mass and frontal structures are easily characterized. For regions without prior highly resolved hydrographic sections (smooth), gridded BGC products (e.g., maps in Koltermann et al., 2011; Orsi & Whitworth, 2005; Olsen et al., 2016), and Argo temperature/salinity properties (http://www.ifremer.fr/co-argoFloats) provide the additional guidance about water mass structure.

The main water masses are identified using potential temperature-salinity-oxygen structure, while the BGC properties assist with identifying relative sources and ages. The first comprehensive A12 occupation with BGC parameters occurred in 1992 as part of the WOCE Hydrographic Programme (WHP). BGC observations have been continued approximately decadally in CLIVAR and GO-SHIP. Vertical sections along A12 are displayed in the Atlantic and Southern Ocean WHP Atlases (Koltermann et al., 2011; Orsi & Whitworth, 2005); a subset is reproduced here with additional labeling (Figure 5). Talley et al. (2011) review the water mass and frontal structure of this region of the South Atlantic, ACC, and Weddell Sea. Orsi et al. (1993), Bakker et al. (2008), and Fahrbach et al. (2011) are foundational sources for Weddell Sea water mass description along A12.

4.2.1. Horizontal Water Mass Structure

The horizontal water mass structure apparent in the 1992 WHP observations along A12 (Figure 5) is characterized by wide zones (i) north of, (ii) within, and (iii) south of the ACC, separated by the narrow SAF and SBDY fronts (Table 2 and sections 4.1.2 and 4.1.4).

(i) The northern region between Africa and the SAF (~45.5°S here) is subdivided by the narrow STF (~39.5°S here), north of which the warmest, most saline upper ocean waters are found (STZ); temperature/salinity/density structures are noisy due to the vigorous Agulhas eddy field (one Agulhas ring evident at 37.5°S). The STF extends to the bottom, as does the ring. Between the STF and SAF, the quieter water mass structure is the Subantarctic Zone (SAZ).

(ii) The ACC begins at the SAF, with its strongly sloped isopycnals and identified by the presence of the salinity minimum Antarctic Intermediate Water (AAIW) north of the front. The PF, within the ACC, is located near 50°S, marked by the northernmost location of a shallow temperature minimum layer; on this A12 section the PF lies above the peak of the mid-ocean ridge complex. The SACCF marks shoaling of the oxygen minimum to about 200 m and southern terminus of the temperature maximum 2 °C contour, which here lies at 51°S in the middle of the ridge complex. The SBDY is at about 57°S on A12, on the southern flank of the bottom ridge complex; it is best developed below the pycnocline and marks the southern terminus of the upwelled deep waters characterized by low oxygen, high salinity, and high nutrients.

(iii) In the Weddell Gyre south of the ACC SBDY, the A12 temperature and density structure is split across Maud Rise. Upward domed contours of the cyclonic Northern Weddell Gyre are found north of the rise. Isolated near-surface temperature and salinity maxima occur over the Rise, which are advected into the Weddell from the northeast, and contribute to the rare multidecadal occurrence of a polynya over the Rise (sections 4.1.3 and 5). South of Maud Rise, the narrow ASF is close to the southern edge of A12, with strong isopycnal slopes indicating westward geostrophic vertical shear.

4.2.2. Vertical Water Mass Structure

(i) In the northernmost region (STZ between Africa and the STF), the water mass structure is that of a subtropical gyre, with additional deep water features associated with the African coast. The Agulhas and Benguela Currents meet and mix in this region, so water properties are complicated. From surface to deep, the main layers are the warm, saline upper ocean (pycnocline) waters with low oxygen that is likely introduced from the Indian Ocean via the Agulhas but might include local production; Antarctic Intermediate Water (AAIW) (salinity minimum); Upper Circumpolar Deep Water (UCDW; oxygen minimum and nitrate/dissolved inorganic carbon [DIC] maximum) that originates as Pacific and Indian Deep Water; North Atlantic Deep Water (NADW; salinity maximum, oxygen maximum, nitrate, and silicate minimum); and cold, dense Antarctic Bottom Water (AABW) that is warmer and saltier than the

newest AABW in the Weddell Sea south of the ridge complex. NADW is most concentrated in an eastward plume rounding the African boundary; it originates as an eastward flow across the South Atlantic, separating from the South American coast at 20–25°S and flowing eastward across the Atlantic to the African coast (Garzoli et al., 2015; Reid, 1994; Tamsitt et al., 2017; Tsuchiya et al., 1994; van Sebille et al., 2012). A SOCCOM float deployed in this STZ could go either westward into the Atlantic or eastward toward the Indian (see 1,000-dbar circulation in Reid, 1994).

The vertical water mass structure in the SAZ between the STF and SAF is the typical higher-latitude Southern Ocean subtropical structure: warmer, saltier at the surface overlying a strong AAIW salinity minimum. The SAZ, unlike the STZ, is characterized by deep penetration of high oxygen and chlorofluorocarbons, to 1,000 m, through the upper ocean and the AAIW layer. AAIW in this sector is a well-ventilated, high-oxygen water mass that originates from Drake Passage to the west (Naveira Garabato et al., 2009; Suga & Talley, 1995; Talley, 1996). The UCDW oxygen minimum at about 1,500 m originates from the low-oxygen Pacific and Indian Deep Waters that enter the Atlantic through Drake Passage; how UCDW leaves the SAZ and upwells across the ACC to the sea surface (Tamsitt et al., 2017) is critical to the question of the Southern Ocean's role in the carbon and nutrient cycles, since it is the principal source of old, high-nutrient/carbon, low-oxygen water that upwells to the sea surface in the Southern Ocean (Sarmiento et al., 2004; Talley, 2013). Beneath the UCDW, the high salinity and oxygen that mark NADW in the SAZ are less extreme compared with the purer NADW against the African coast. The 1992 A12 section has DIC measurements only in this sector and farther south (Figure 5f) and shows the expected lower values in the lower nutrient NADW. Isopycnals are flattest throughout the water column in this zone. Based on these water masses and on the 1,000-dbar circulation in Reid (1994), we would expect SAZ floats to circulate eastward toward the Indian Ocean.

(ii) Within the ACC, the northernmost region is the PFZ between the SAF and PF. Isopycnals here begin their steep rise toward the south and continue to rise steeply southward through the AZ to the SACCF and SBDY. The PF is the northern limit of the subsurface temperature minimum at about 200-m depth and has a sharp horizontal density gradient directly above the northern peak of the Mid-Atlantic Ridge, signaling strong shear. In terms of water masses, the PFZ otherwise is linked with the AZ, as in Gray et al. (2018). At the sea surface within the PFZ/AZ, the lowest salinities on this summer section are encountered, with the lateral minimum at 53°S (<33.9) coinciding with the SACCF. These low salinities arise from northward sea ice export and melt on the outer edge of the Weddell gyre, at the southern ACC fronts (Abernathey et al., 2016). (Float time series within the Weddell Sea show spring, postmelt surface salinities that are equally low, but the low surface salinity quickly erodes into summer.) Surface layer temperature in the entire PFZ has a large meridional gradient that suggests active warming of the northward flowing Ekman layer (Cerovecki et al., 2011; Tamsitt et al., 2016). The net buoyancy input from freshwater and heating allows upwelled waters to join the surface layer and upper cell of the Southern Ocean overturning circulation here. In the PFZ/AZ, beneath the fresh surface layer, the upwelled UCDW is readily apparent, bringing warmer, saltier, low-oxygen, high-nutrient, and high-carbon water up to 200-m depth, just beneath the strong halocline/pycnocline. Floats in this regime would be expected to circulate eastward.

(iii) In the northernmost Weddell Gyre, just south of the ACC's SBDY and along the southern flank of the America-Antarctic Ridge, is a vertical band of higher oxygen (200- to 600-m depth; Figure 5e) and chlorofluorocarbons (CFCs; 500 to 4,500 m) (Koltermann et al., 2011), marking the northern side of the cyclonic Weddell circulation. We expect floats to move eastward in this northernmost Weddell Gyre zone.

Within the Weddell Gyre, the vertical structure is cold, fresh surface waters separated from the underlying layer by a very strong halocline; a temperature maximum layer that includes an oxygen minimum; cold, nearly uniform salinity Weddell Deep Water (WDW); and the coldest, highly oxygenated, new AABW. The WDW structure domes within the northern Weddell Gyre, between the America-Antarctic ridge and Maud Rise. The oxygen minimum is coincident with the temperature maximum layer here and lies just below the halocline/pycnocline. While the somewhat thick layer of low oxygen between 150 and 600 m is likely due to upwelled oxygen minimum Deep Water, the oxygen minimum close to 150 m is likely due to local biological processes, as shown from these and other SOCCOM floats by Briggs et al. (2018).

On both flanks of Maud Rise, between 200- and 500-m depth, is the warmest and saltiest water in the Weddell Sea on this section; its source is advection from the northeastern Weddell Gyre (Orsi & Whitworth, 2005). The

unique stratification above Maud Rise reflects its well-documented Taylor column and vertical mixing (Bersch et al., 1992), and there was a hope, which was realized (Figure 2b), that floats deployed along A12 would become entrained in this circulation.

Finally, at the Antarctic coast, the downward plunge of all property contours and increases in oxygen and CFCs marks the Antarctic Slope Front, where new AABW spills down the slope. High CFCs in the AABW are found to the bottom in a narrow strip along the coast. Note that Argo/SOCCOM floats, which profile to 2,000 m, cannot observe AABW unless they are in the narrow downward plume of AABW at the continental shelf. These features are very difficult to sample with floats, so the goal with floats in this region was to launch them in the westward flow that continues on into the Weddell Sea, rather than an attempt to sample new AABW.

To summarize, based on these water properties, we assigned at least one float in each of these regimes: the STZ north of the STF, the SAZ between the SAF and STF, the PFZ/AZ between the SAF and SACCF, the SoZ between the SACCF and SBDY, the Weddell gyre circulation just south of the SBDY, the central Weddell gyre between Maud Rise and the SBDY, Maud Rise, and the continental shelf boundary flow.

4.3. A12 Predeployment Trajectory Analysis

Predicting the possible pathways of SOCCOM floats using quasi-Lagrangian information is an essential tool for deployment strategy. From a practical perspective, we needed to project which floats would require ice avoidance software (which was not available on all floats at the start of SOCCOM) and wished to avoid floats drifting into regions of multiyear sea ice.

Projection of the most likely float pathways requires a large ensemble of prior trajectories. Prior Argo floats provide an observationally based guide to dispersion in this region, but the number of prior floats limited this approach, especially in the sea ice zone. Modeled float releases provide many more trajectories but are simulations. Both actual Argo trajectories and model simulations are based on a prior ocean state under different forcing than actually occurs after float deployments, introducing additional uncertainty. In section 5.1 we compare the projected track ensembles with the actual PS89 SOCCOM float tracks.

During PS89 float planning, we examined historical Argo floats from south of 50°S that included 27 floats from the University of Washington in the Weddell gyre (Chamberlain et al., 2018), hence under sea ice part of the year, as well as all historical tracks within the ACC (supporting information Figure S1a). (For current SOCCOM planning, we use all available Argo trajectories.) The Argo trajectories delineated the two southern ACC fronts crossing the PS89 section. Floats originating in the Scotia Sea swing northward around the Scotia Ridge and then southward along its eastern side, splitting to enter the two fronts. These floats and fronts then trend northeastward along the northern side of the Weddell Sea, crossing the PS89 section, following the American-Antarctic and Southwest Indian Ridge. The fronts and prior floats move away from the ridge at its fracture zones at about 20°E and shift southward with large mesoscale variability between 20° and 40°E. South of the ridge, sea ice is present in winter (straight, linearly interpolated float tracks in supporting information Figure S1a). Even with limited float coverage, the generally cyclonic Weddell Gyre circulation is apparent, with the strongest currents close to the Antarctic shelf, as in Fahrbach et al. (2011). In the previous 2001–2014 float deployments in Figure S1a, floats released south of about 67°S entered multiyear ice regions. Therefore, we planned no SOCCOM releases at the southernmost A12 and southwesternmost Weddell Sea PS89 stations.

With synthetic (modeled) floats used as an observing system simulation experiment (OSSE), potential pathways can be probed more thoroughly. SOCCOM uses both SOSE (Mazloff et al., 2010) and the Hybrid Coordinate Ocean Model (HYCOM) (Bleck, 2002) to simulate possible float trajectories. We tested all the planned, closely spaced PS89 stations as potential deployment locations. (For simulations for SOCCOM cruises without preplanned, closely spaced stations, test locations are chosen with approximately 100-km spacing along the cruise track.) SOSE (http://sose.ucsd.edu) is a 1/6° state estimate for the region south of 30°S, constrained by available in situ observations and forced with National Centers for Environmental Prediction (NCEP) reanalysis; several runs, with output archived on the website, are available. Prior to SOCCOM deployments, the archived version was SOSE iteration 66, which covered years 2005–2006. At time of analysis for this manuscript, several years after deployment, the best version was SOSE iteration 100, covering years 2005–2010. For postdeployment analysis we therefore use SOSE iteration 100. SOSE is described extensively elsewhere (Mazloff et al., 2010; Verdy & Mazloff, 2017) and is used for many Southern Ocean

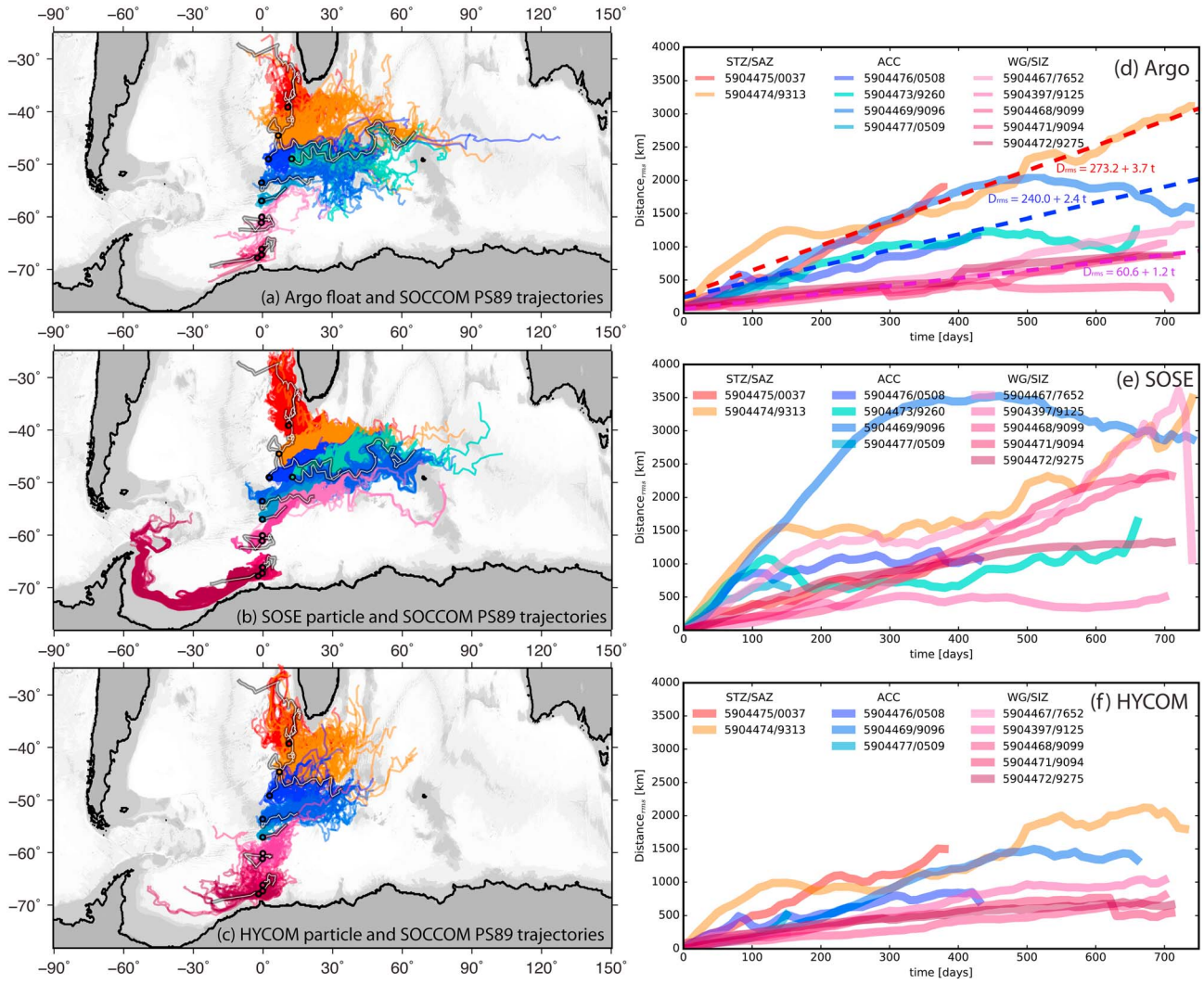

Figure 6. (a–c) Float trajectory maps, each panel including SOCCOM PS89 trajectories (heavy lines with white core) through October 2017: (a) Argo float trajectories that pass through 2 × 2° range of actual PS89 float deployment, tracked to maximum time of SOCCOM trajectory as of October 2017, or until they die if trajectory is shorter. (b) SOSE-simulated float trajectories. The cluster at each SOCCOM float deployment location represents 365 synthetic floats, released one per day for a year, starting 1 January 2005 and followed for 3 years. (Supporting information Figure S1b shows the SOSE simulation used for planning purposes, including all PS89 stations, and a different release protocol.) (c) HYCOM-simulated float trajectories, for 2 years, starting at each planned station location. (d–f) Postdeployment trajectory analysis, using SOCCOM float trajectories for November 2014 to February 2017. RMS difference distance between actual SOCCOM float trajectories (UW ID numbers) and (d) Argo float trajectories, (e) SOSE-simulated floats, and (f) HYCOM-simulated floats. (As float 5904473/9260 location was added during the cruise, there is no associated HYCOM simulation.) See also supporting information Figures S1 and S2.

analyses; a 1/12° version extending to more recent years is becoming available. The HYCOM OSSEs use velocities from a global data-assimilating HYCOM climatological simulation with 1/12° horizontal resolution (simulation GLBa0.08, http://www.hycom.org).

Simulated floats in SOSE (Figure 6b) used the *Octopus* module developed by J. Wang (e.g., Tamsitt et al., 2017; van Sebille et al., 2018). The synthetic float movement mimicked Argo floats with parking at 1,000 m and profiling 0–2,000 m every 10 days, assuming a constant profiling speed (−0.047 m/s descending and 0.055 m/s ascending). At the time of precruise planning, only SOSE iteration 66 was available; because the model run covered only 2 years, the output was looped three times to provide a 6-year velocity field. For postdeployment analysis (Figure 6b), SOSE iteration 100 (2005–2010) was available and did not require looping because of the greater length of the model run. Each planned PS89 station had a cluster of 2,000 synthetic floats randomly distributed within a 1/3° box, 200 of which are shown from the February run for each cluster (supporting information Figure S1b). For the postdeployment

SOSE simulation (Figure 6b), one float was released per day for 365 days at the SOCCOM float deployment location and was followed for 3 years.

For the HYCOM OSSE (Figure 6c and supporting information Figure S1c), an ensemble of trajectories was created by releasing particles at each of the 40 stations, but varying the deployment starting date in 8-day increments, with a maximum deviation from the actual proposed starting date of 32 days (nine releases per station). The procedure was repeated for 5 years within the 2010–2013 interval, and the synthetic floats were followed until the end of year 2014. Each simulated HYCOM float was parked at 1,000-m depth for 9 days, then descended to 2,000 m, ascended to the surface over 12 hr, and finally descended back to the 1,000 m over the next 12 hr. (About 1 day of each 10-day cycle is spent profiling, for both the actual and simulated floats.) Depth-averaged velocities were used to advect synthetic floats during their ascent and descent.

The simulated floats from both OSSEs show four major regimes of differing zonal flow direction along the A12 section: (i) westward for the northernmost release positions (west of the Agulhas retroflection), (ii) eastward between 41°S and 61°S (ACC and subtropical gyre), (iii) variable eastward or westward between 61°s and 65°S (northern Weddell Gyre), and (iv) westward south of 65°S (Maud Rise and the ASF or southern limb of Weddell Gyre). The reversal between westward and eastward flows at 65°S is especially sharp. SOSE trajectory ensembles, especially those south of 60°S, have less mesoscale (eddy) variability and extend farther from the release locations than HYCOM trajectories, likely due to inadequate mesoscale resolution in the 1/6° SOSE. ACC particles tend to aggregate in frontal flows, particularly the SBDY (58°S), which is pinned to the underlying topography, the SACCF (~52°S), the SAF (~48°S), and a less well-defined Agulhas Return Current that joins farther east at Kerguelen with the SAF, which is a well-known feature of Indian Ocean circulation (e.g., Figure 11.1 in Talley et al., 2011). SOSE floats released in the SAF travel farthest eastward, past Kerguelen, in the 6-year simulation. The HYCOM experiments exhibit a larger ensemble spread because the deployment date was varied and the model has higher resolution than SOSE, but the dispersion is similar: HYCOM floats deployed south of 65°S move preferentially (more than 70%) westward into the Weddell Sea. HYCOM floats released between 58°S and 65°S do not move far and move variably east and west, with a slight preference to go east (>65%). Floats released between 48°S and 58°S follow a southern path eastward into the Indian Ocean. Floats between the third station and 48°S follow a northerly path eastward into the Indian Ocean. Floats from the northernmost two stations are likely to end up in the Benguela region, although a group of particles ends up in the Indian Ocean.

Multiyear sea ice avoidance has been a requirement for at least the first year of SOCCOM floats. Floats released in the interior Weddell Gyre at all A12 stations should be good choices based on the OSSEs. On the other hand, floats released from the southern set of cross-Weddell (A23) stations could quickly enter the multiyear ice regime, so these locations should be avoided. (In actuality, the Polarstern did not occupy these stations, and so this information will be applied to the next Polarstern cruise, PS117, in 2018–2019.) These OSSE results support expectations based on the limited historical Argo trajectories in the Weddell Gyre (Figures 6a and S1a).

4.4. SOCCOM Float Deployment Choices for PS89

The final deployment plan for 12 floats along the A12 section and crossing the Weddell Sea included one or more floats in each regime (Table 2), taking circulation and multiyear sea ice into account. We interspersed the four novel Seabird Navis floats with the eight Apex floats, with an Apex float backup for each Navis float in a given regime except in the STZ (Navis only). Nearly coincident deployments with French BGC-Argo PROVOR floats in the STZ, SAZ, and PFZ showed that the three different particulate backscattering sensors produced significantly different values, with the source of the differences not yet understood, although all showed a seasonal cycle at depth in the biologically active PFZ (Poteau et al., 2017).

Deployment locations are shown on the maps in Figures 2–4 and indicated in Figure 5a. From north to south, planned deployments of our 12 floats were one float each in the STZ, the SAZ, the PFZ, and the SoZ; three floats in the Northern Weddell Gyre (NWG) and Maud Rise region; one float between Maud Rise and the ASF, far enough south for westward flow but north of the multiyear ice; and four floats at the northwestern Weddell Sea stations. A tradeoff was that no float was planned for the AZ between the PF and the SACCF. When the four interior Weddell Sea deployments were canceled due to ship malfunction, alternative locations along the return transit to Cape Town were selected: one (ASF 5904472) as far southwest as possible

to improve chances of a float moving westward into the Weddell Sea, one (MR 5904468) close to Maud Rise to back up Navis MR 5904478, one (NWG 5904397) in the Northern Weddell Gyre close to NWG 5904467 to provide pH measurements and back up Navis 5904477, and one (5904473) in the PFZ to provide pH measurements and back up Navis float 5904476. Thus, we deployed in seven of the nine regimes (Table 2), missing the AZ (weather) and the interior Weddell Sea (ship malfunction).

5. PS89/A12 Deployments and Outcomes

5.1. RV Polarstern PS89 Float Deployments and Performance

RV Polarstern departed Cape Town on 2 December 2014 and reached Atka Bay (Neumayer Station III) on 25 December, having completed mooring recoveries and deployments, CTD stations, and eight SOCCOM float deployments (Figure 2). A malfunction of a propeller control system in heavy ice prevented the Polarstern from continuing on across the Weddell Sea to Punta Arenas. The ship was rerouted back to Cape Town, departing Atka Bay on 13 January 2015 and arriving in Cape Town on 1 February 2015 (Boebel, 2015). The last four SOCCOM floats intended for the Weddell Sea were deployed on the northward transit (section 4.4). The southernmost float became the only one to move westward into the interior Weddell Sea where it has now undergone three annual cycles (section 5.2).

At every float deployment location, a shipboard profile was collected, including CTD temperature/salinity/oxygen and fluorescence/backscatter profiles and discrete salinity, oxygen, nutrients, pH, alkalinity, DIC, HPLC, and POC measurements. SOCCOM floats are deployed just after completion of the CTD station, after pulling away slowly at approximately 1 knot from the station location to reach clean water. The first reported float profile is approximately 18 hr later, but this is not problematic because shipboard data are used for statistical validation rather than individual sensor calibration (Johnson, Plant, Coletti et al., 2017).

Of the 12 floats, the 8 Apex floats functioned as expected, equivalent to the success rate of the global core Argo fleet (Riser et al., 2018), and 7 are currently providing data past their third winter cycles. One Apex float worked for 66 profiles (PFZ float 5904473) but lost buoyancy and hence telemetering capability in December 2016. Of the four Navis floats, only STZ float 5904475 is still providing data, despite a midlife mechanical profiling failure for 20 profiles that self-corrected; the float has since provided more than 60 full profiles. Our strategy to intersperse Apex and the novel Navis floats was therefore appropriate for maintaining coverage of as many oceanic regimes as possible, while testing the new float design. The Navis float buoyancy engine was subsequently redesigned, and thereafter, the SOCCOM Navis floats have had no mechanical failures (Riser et al., 2018). Thus, the plan for ~200 BGC floats in the Southern Ocean is on track and expected to be successful. We note that this goal is more than sufficient for reconstruction of the annual mean oxygen and DIC, based on Kamenkovich et al. (2017), and so our goal of 200 includes redundancy.

Oxygen, nitrate, chlorophyll, and backscatter sensors functioned as expected on all 12 floats. Five pH sensors continue to perform well. Two floats (northern Weddell Gyre or NWG 5904467 and STZ 5904475) had no pH sensors originally; the pH sensor on PFZ 5904476 failed soon after deployment; four other pH sensors failed before the end of float lifetime. These novel pH sensors have been successfully redesigned (Johnson, Plant, Coletti et al., 2017).

5.2. Trajectory Analysis Evaluation for A12 SOCCOM Floats

Here we evaluate the use of prior Argo trajectories and SOSE- and HYCOM-simulated float trajectories for the A12 Polarstern SOCCOM float deployment strategy. Note that SOCCOM BGC-Argo floats follow the same profiling mission as Argo floats (section 1).

Argo float trajectories from all years that passed within a 1° latitude/longitude bin around each A12 SOCCOM float deployment are shown in Figure 6a, with the SOCCOM trajectories as of July 2017 superimposed. The Argo float trajectories were qualitatively skillful in predicting potential trajectories for the SOCCOM floats. SOCCOM floats deployed in the core of the ACC (PFZ and SOZ) advected rapidly to the east along a high float density route followed by prior Argo floats. The five SOCCOM trajectories in the Weddell Gyre (regions 6–8 in Table 2) were reasonably well predicted for eastward, westward, or minimal flow, despite the small number of floats prior to SOCCOM. The biggest difference relative to historical Argo was for floats in the energetic northern regime. The northernmost STZ 5904475 float's northwestward trajectory into the Benguela region was not unexpected, although it could instead have gone eastward in the Agulhas retroflection. On the other

hand, SAZ 5904474 did not follow an expected eastward path but jumped northward across the STF where it remained trapped in the eastern Cape Basin until September 2017, after which it has joined the eastward Agulhas Return Current. Overall, with this exception, the prior Argo float trajectories were informative for the very sparse SOCCOM deployments, even where Argo itself is sparse, as in the Weddell Gyre.

To assess the predictability of the individual SOCCOM trajectories, Figure 6d shows the RMS distance as a function of time between each float location and all historical Argo floats that passed through that SOCCOM float's 1° deployment gridbox, for the 11 SOCCOM tracks that are continuous and longer than 170 days:

$$D_{rms}(t) = \left[\frac{1}{N}\sum_{iP-1}^{N}\left(\overline{x}_{SF}(t) - \overline{x}_{iP}(t)\right)^2\right]^{1/2} \quad (1)$$

where $\overline{x}_{SF}(t)$ is the SOCCOM float position at time t and $\overline{x}_{iP}(t)$ is the position of the ith Argo float or simulated float in the ensemble of N Argo floats. (STZ 5904475 is not included beyond 68 profiles because surface currents carried it across the Walvis Ridge during a 20-profile gap.)

After 1 year, Argo-SOCCOM RMS distances grew to ~1,350 km in the subtropics (Agulhas-dominated), 875 km in the ACC, and 440 km in the Weddell Gyre (Figure 6d). While the individual tracks of the northern STZ/SAZ floats (5904475 and 4904474) appeared unusual, their large relative dispersion is consistent with the high subtropical lateral diffusivity estimated previously from profiling floats (Davis, 2005).

The ACC floats had lower relative dispersion, compared with Argo, than the subtropical floats, also consistent with Davis's (2005) distribution of diffusivity. The one ACC outlier, SoZ 5904469, was trapped south of Spiess Rise at the topographic triple junction, within 1° of launch site, for its first 45 profiles (450 days, so 15 months), after which it moved quickly eastward following the Southwest Indian Ridge and then southward into the Weddell Gyre. Once it left the launch site, its behavior was more typical of the Argo ensemble.

The five Weddell Gyre floats, including the southernmost float in the fast, westward ASF, dispersed least from the historical Argo trajectories. MR 5904468 was trapped over Maud Rise in a Taylor column (Figure S4) and diverged least from the historical floats; thus, previous floats deployed here have also lingered near Maud Rise. This is encouraging for future float planning, given the central importance of Maud Rise in decadal winter polynya formation and water mass transformation.

SOSE-simulated floats (Figures 6b and 6e) show reasonable predictive skill relative to the A12 SOCCOM trajectories, but with less clear regime (northern, ACC, Weddell) distinctions than historical Argo trajectories. Neither historical Argo nor SOSE floats suggested a high likelihood that SAZ 5904474 would jump across the STF to enter the STZ, which was a loss for our regional sampling strategy. Having jumped across the STF, SAZ 5904474 behaved like the SOSE-simulated float ensemble and was trapped in the Cape Basin's vigorous mesoscale field north of the Agulhas Ridge, which guides the STF here. While the westward propagation of Agulhas rings and eastward retroflection into the Agulhas Return Current are the usual focus of regional analyses (Gordon, 2003; Richardson, 2007), the dominant behavior here is retention (trapping), well known to regional specialists (Speich, personal communication). This may be due to movement of Lagrangian objects toward high eddy kinetic energy (e.g., Davis, 1991; Freeland et al., 1975; LaCasce, 2008), which can be expressed in terms of the spatial gradient of the lateral diffusivity.

In the ACC, the SOSE-simulated ensemble had a particularly wide spread, with groups of simulated floats separating to follow different fronts eastward (PF and SACCF/SBDY), whereas the ensemble of historical Argo floats passing through each SOCCOM float deployment location was more strongly constrained by topography. This suggests that topographic control in the 1/6° SOSE is too weak. SoZ float 5904469, which observed the unexpectedly large and highest surface carbon outgassing signal in this entire set of 12 SOCCOM floats (Gray et al., 2018), diverged even more from SOSE-simulated floats than from historical Argo floats.

In the Weddell Gyre, the 1/6° SOSE does not show trapping over Maud Rise, which differs from SOCCOM and historical Argo floats. A second major discrepancy is in the ASF, where SOSE simulated floats zoom westward but SOCCOM float ASF 5904472 and historical Argo floats are much slower. Neither SOCCOM nor historical floats show much eddy variability in the ASF during tracked, open-water periods (supporting information

Figure S1a). The discrepancy in speed is likely due to inability of the 1/6° model to capture steady, narrow currents, including those steered by topography.

HYCOM-simulated floats (Figures 6c and 6f) were more skillful than the lower resolution SOSE in projecting SOCCOM trajectories. HYCOM represents all three major relative dispersion regimes captured by Argo, but HYCOM dispersion (related to the slope of D_{rms}) is lower than for Argo. HYCOM performed better than SOSE for the northernmost STZ 5904475 and SAZ 5904474 and for the southernmost ASF 5904472. HYCOM, unlike SOSE, shows float trapping at Maud Rise. The importance of high spatial resolution at high latitudes is relevant as SOCCOM and the new UK ORCHESTRA program are planning future Weddell Sea float deployments, and models such as HYCOM and SOSE are used to inform deployments.

The purpose of the D_{rms} calculation was to evaluate the use of Argo and modeled synthetic floats in predicting dispersion of our individual floats. This dispersion quantity (equation (1)) is related to the Lagrangian relative diffusivity, which requires averaging (1) over many individual floats, but which we are not doing here. Davis (2005) mapped the diffusivity using WOCE profiling floats; magnitudes were similar to those from surface drifters (Zhurbas & Oh, 2004). Both show large diffusivity in the STZ/SAZ (Agulhas retroflection variability) ($10–30 \times 10^3$ m^2/s), medium diffusivity in the ACC (~3×10^3 m^2/s), and lowest diffusivity in the Weddell Gyre (~1×10^3 m^2/s). This matches our observation of largest relative dispersion in the STZ/SAZ and smallest in the Weddell (Figure 6d). In supporting information Figure S2 and Text S1, we use the SOCCOM-Argo variance D_{rms}^2 to crudely estimate two-particle relative diffusivity, following Klocker et al. (2012). However, because our focus is on evaluating this set of SOCCOM floats rather than making a full diffusivity calculation, we average over only the few floats in each of the three large regimes relative to the full Argo data set, instead of using the full Argo trajectory data set to calculate the best estimates of variance. Nevertheless, the southward decay is encouragingly similar to Davis (2005). Thus, published diffusivity distributions are useful for assessing potential SOCCOM float deviation relative to the ensemble of all historical Argo floats.

5.3. Oceanic Regime Coverage by A12 SOCCOM Floats

We briefly summarize water property regimes covered by the PS89 SOCCOM floats with more than 20 profiles: (i) in the STZ and SAZ north of the ACC, (ii) within the ACC, and (iii) in the sea ice zone of the Weddell Sea. Two examples are illustrated in Figure 7: (i) the SoZ *chimney* float (SoZ 5404469) within the ACC that contributed to Southern Ocean outgassing carbon flux (Gray et al., 2018; Williams et al., 2017) and (ii) the southernmost under-ice float in the ASF (ASF 5404472). Trajectories and additional parameters (pH, derived DIC, and derived alkalinity) for these two floats are shown in supporting information Figures S3 and S4.

The following discussion of how well these floats sampled the desired regimes is detailed but qualitative. Now that the SOCCOM array is growing, quantitative work on evaluating our success in sampling the many biogeochemical regimes has been started, using methods such as k-means clusters (e.g., Ardyna et al., 2017) and evaluation in biogeochemical Southern Ocean State Estimate.

5.3.1. Subtropical and Subantarctic Zone Floats (Also Supporting Information Section S2.1)

Two PS89 floats (STZ 5904475/0037 and SAZ 5904474/9313) have sampled the STZ/SAZ throughout, and one (PF 5904473/9260) started in the PFZ, followed by the SAF, and crossed into the SAZ at the end of its lifetime. Detailed description is in supporting information section S2.1.

The northernmost STZ float 5904475 was deployed in the Cape Basin north of the Agulhas Ridge, a highly energetic, eddy-rich region just west of the Agulhas retroflection (Gordon, 2003;Richardson, 2007). Water properties in this Agulhas-influenced region were partially SAZ with a transition to STZ. STZ 5904475 then became stuck at the surface for 19 cycles and was advected by surface currents westward over the Walvis Ridge where it began to profile again. It is currently in the South Atlantic's subtropical gyre, sampling properties illustrated by the Atlantic A10 section and the subtropical portion of A16 (Koltermann et al., 2011; Tsuchiya et al., 1994).

The second northern float, SAZ 5904474, was deployed in the SAZ south of Agulhas Ridge but crossed the topographic ridge-guided STF after profile 45 (19 September 2015) then entered and stayed in the subtropical Cape Basin for 2 years through profile 115 (1 September 2017), after which it joined the Agulhas Return Current and has been moving east (section 5.2). As a result, we lost coverage of the SAZ in this Atlantic sector, which was later remediated with SOCCOM deployments in mid-2017 (Table 1, Cruise 17). In the SAZ, the salinity structure included freshest water at the surface, a salinity maximum at about 300 m, and an AAIW salinity

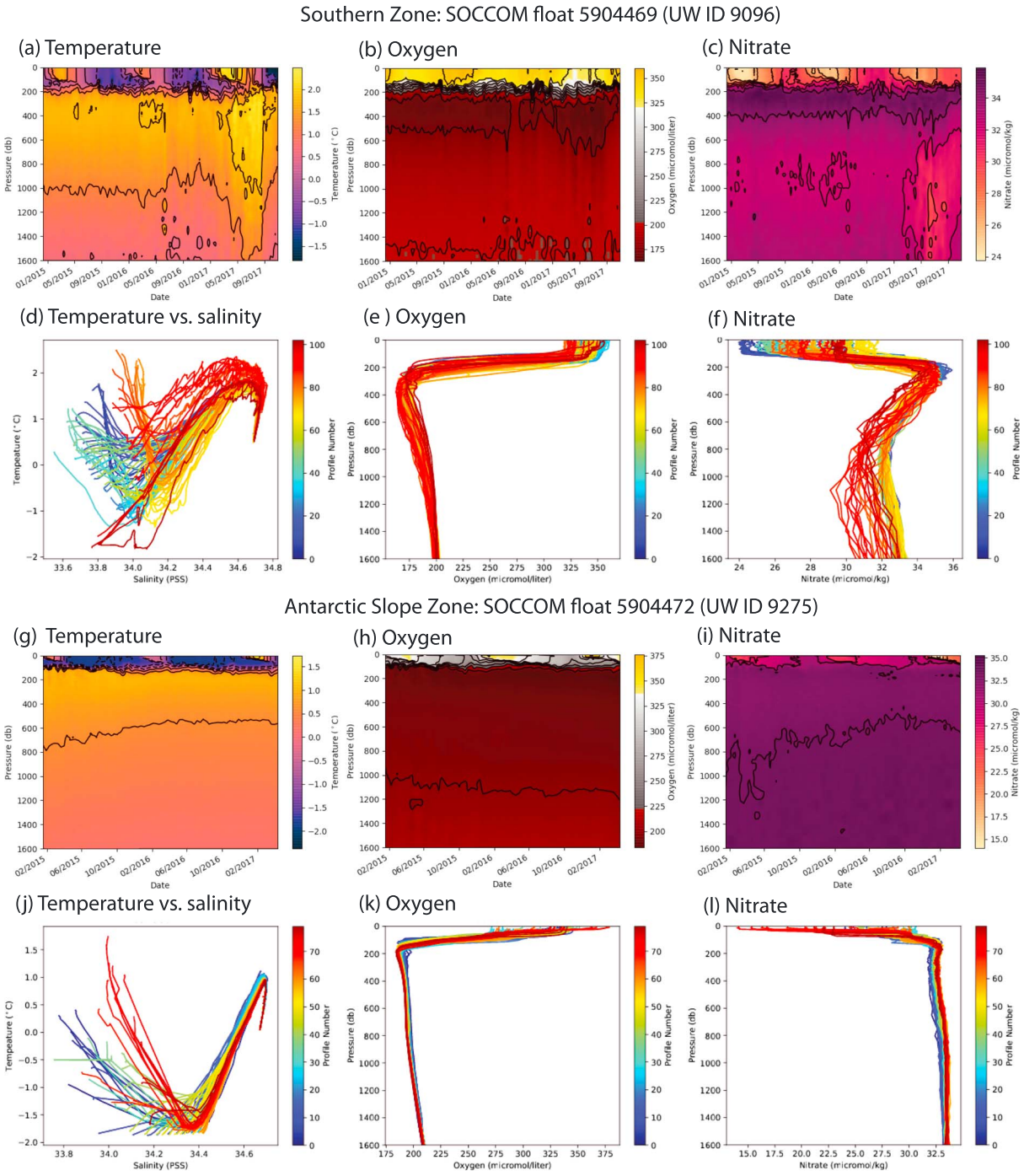

Figure 7. Time series and profiles from two representative SOCCOM floats deployed from PS89 ANT-XXX/2 (WMO ID 5904469/UW ID 9096—Southern Zone; WMO ID 5904472/UW ID 9275—Antarctic Slope Front): (a, g) potential temperature (°C), (b, h) oxygen (μmol/kg), (c, i) nitrate (μmol/kg), (d, j) potential temperature versus salinity, (e, k) oxygen (μmol/kg), and (f, l) nitrate (μmol/kg). See supporting information Figures S3 and S4 for additional properties from these floats.

minimum shallower than 500 m, while oxygen structure included a 500-m maximum associated with AAIW and 1,400-m minimum associated with Pacific Deep Water/Indian Deep Water. The property jump across the STF is clear in potential temperature, salinity, oxygen, and nitrate. The float's STZ *Cape Cauldron* (Gordon, 2003) structures result from mixing of upper waters from multiple sources. When the float moved northward all the way to the African coast, it sampled near-coastal Benguela waters and its near-surface oxygen dropped precipitously, typical of this very productive region. Since May 2018, this float has been

within the Agulhas Return Current, with a much deeper thermocline, warmer, saltier upper ocean, and much deeper Indian Deep Water core (high nitrate and low oxygen). Until expected SOCCOM float deployments in the Agulhas in 2019, this is SOCCOM's only Agulhas float.

5.3.2. Antarctic Circumpolar Current Floats (Also Supporting Information Section S2.2)

There are three zones within the ACC: the PFZ, AZ, and SoZ, from north to south. Two floats were deployed in the PFZ (5904476 and 5904473) and two in the SoZ (5904496 and 5904477), but none in the AZ. SoZ 5904477 completed only 17 profiles. SoZ 5904496, which is the carbon-outgassing float on PS89 (Gray et al., 2018; Williams et al., 2017), is described here. Details for the others are in supporting information section S2.2.

PFZ 5904476 and 5904473, both deployed nominally south of the SAF, were drawn into the swift, eastward SAF and fluctuated between SAZ and PFZ properties. The Navis float (PFZ 5904476) was deployed along the Good Hope section, while the Apex float (PFZ 5904473) was deployed to the east. The eastward track of the Navis float overlapped with the Apex float, and they can in some sense be considered as a single trajectory within the SAF, given the premature end of PFZ 5904476's profiling. The SAF has a major permanent northward meander around Crozet Bank at 50°W, which has been followed by many Argo floats and also by PFZ 5904476. Temperature became warmer during this loop and downstream path to Kerguelen Plateau at 60°W, where the float encountered the southeastward flow of the warm, saline Agulhas Return Current, resulting in enormous temperature/salinity interleaving. On these PFZ floats, the oxygen minimum and carbon maximum were relatively deep. The wind stress curl is also close to zero, with annual mean downwelling along these floats' pathways. Both factors likely contributed to their small net annual air-sea carbon flux, compared with the large ocean carbon outgassing observed on the next float to the south, SoZ 5904496, discussed next.

SoZ float 5904496 (UW ID 9096; Figures 7a–7f) was deployed between the SACCF and SBDY, just north of the Bouvet triple junction where the Southwest Indian Ridge, Mid-Atlantic Ridge, and America-Antarctic Ridge meet. This is PS89's *chimney float*, tracking low-oxygen/high-carbon deep waters that rise to just beneath the winter mixed layer (section 4.2). The first two annual cycles of this float showed large winter CO_2 outgassing, contributing to the newly documented, robust signal of circumpolar outgassing in the ACC (Gray et al., 2018; Williams et al., 2017). For its first 46 profiles (460 days), SoZ 5904496 was trapped within 1° latitude/longitude, circulating anticyclonically around Spiess Seamount, after which it broke loose and moved quickly eastward in the SACCF along the Bouvet Fracture Zone. It jumped to Shaka Fracture Zone at profile 56 and then closely followed the crest of the Southwest Indian Ridge. Up to this point, the float was in the SoZ, north of the winter sea ice, with cold but not freezing surface water. After 81 profiles, SoZ 5904496 entered a region of high mesoscale variability at a break in the Southwest Indian Ridge, where ACC water moves cyclonically south and southwestward to enter the Weddell gyre. As it has progressed along this southwestward route, its temperature maximum at about 500-m depth has warmed and its oxygen/nitrate minimum/maximum has become lower/higher. This suggests that it is now sampling the inflow of the northern Deep Waters that penetrate upward across the ACC and enter the Weddell gyre (e.g., Bakker et al., 2008).

5.3.3. Weddell Gyre Floats (Also Supporting Information Section S2.3)

Six floats were deployed in the Weddell gyre: two in the northern Weddell gyre (NWG 5904397 and 5904467), three west of Maud Rise (MR 5904471, 5904468, and 5904478), and one close to the Antarctic Slope Front (ASF 5904472). The ASF float is detailed here (Figure 7); the others are detailed in supporting information section S2.3.

NWG 5904397 and 5904467 have three under-ice seasons thus far, tracing the local cyclonic circulation in this subbasin (Fahrbach et al., 2011). Although MR 5904471, 5904468, and 5904478 (four profiles only) were deployed west of Maud Rise, they moved up onto the rise and into a Taylor column, where they have sampled an extraordinary opening of the Maud Rise polynya in 2016 and 2017, which evolved to a larger Weddell Polynya in 2017 Polynya (Swart et al., 2018) that has been nearly as intense as the notable 1974–1976 polynya (Gordon, 1978; Gordon et al., 2007). Climate forcing related to these major polynya events included a strong positive Southern Annular Mode in 2015 and 2016 (Swart et al., 2018). Also potentially associated was a positive phase of the quasi-biennial oscillation (QBO) for the two polynya years (2016 and 2017; not shown). Both the positive SAM and positive QBO strengthen the zonal westerlies and create a tendency for stronger cyclonic winds over the Weddell Sea. (Additional description of the MR floats is provided in supporting section S2.3 and Figure S4.)

The farthest south ASF 5904472 (Figures 7g–7l) is the only PS89 float that has moved westward into the main Weddell gyre. Its trajectory was predicted well by Argo, HYCOM, and SOSE and its speed by Argo and HYCOM. It has emerged from its third winter (profiles 9–23, 44–67, and 81–107 under ice) and is now back under ice for a fourth winter. The temperature and salinity profiles are classically Weddell gyre: cold, fresh surface layer, strong pycnocline at ~100-m depth and subsurface temperature and salinity maxima at ~200-m depth. Oxygen/nitrate also has a pronounced minimum/maximum at 200 m, reflecting local respiration/remineralization (e.g., Briggs et al., 2018). This surface structure becomes progressively colder and more saline along the westward path, likely due to sea ice production. The temperature maximum on the last set of profiles in late 2017 is colder and the vertical structure noisier, suggesting active mixing. Derived DIC at the DIC maximum (supporting information Figure S5) increases westward, possibly due to carbon accumulation through the biological pump. More discussion and figures are in supporting information section S2.3.

6. Summary

The deployment of 12 SOCCOM BGC-Argo floats in late 2014 and early 2015 from RV Polarstern PS89 was the second such deployment by our group, following deployment of 12 floats from RVIB N.B. Palmer during GO-SHIP P16S in early 2014 and was the first deployment within SOCCOM funding. SOCCOM is implementing sparse coverage of the entire Southern Ocean. Deployment strategy is guided by water mass regimes and circulation. Knowledge thus acquired prior to each SOCCOM cruise has been invaluable in adapting in real time to individual cruise and float situations.

Water mass regimes were usefully identified for PS89 using WHP hydrographic properties and surface climatologies; we now incorporate existing Argo and our growing SOCCOM BGC-Argo data sets. Circulation features and variability were identified using prior Argo float trajectories and OSSEs using particle releases in high-resolution state estimation (SOSE) and data-assimilating simulations (HYCOM).

The PS89 floats have already been used with the other SOCCOM floats with full annual cycles of nitrate, pH, and oxygen in circumpolar syntheses of climatological seasonal cycles (Williams et al., 2018), net community production (Johnson, Plant, Dunne et al., 2017), air-sea carbon flux (Gray et al., 2018; Williams et al., 2017), and air-sea oxygen flux (Bushinsky et al., 2017), respectively. The two PS89 floats trapped at Maud Rise (MR 5904471 and MR 5904468) were serendipitously in place to sample the noteworthy opening of the Maud Rise/Weddell polynya in austral winters 2016 and 2017 (Swart et al., 2018). Ocean color satellite matchups are being used to test the NASA ocean color algorithms for chlorophyll and POC (Haentjens et al., 2017). Our growing array is also providing good coverage of Southern Ocean bioprovinces (Ardyna et al., 2017) and will be interesting to analyze in those terms.

The SOSE- and HYCOM-simulated float OSSEs reasonably projected the circulation and were invaluable for locating sharp fronts, but postdeployment analysis shows that historical Argo trajectories are the most useful. All were more useful than qualitative use of mean circulation analysis or one based solely on altimetry. HYCOM underpredicted and SOSE overpredicted the spread of float trajectories compared with Argo and SOCCOM floats, and SOSE did not cleanly distinguish the three major dynamical regimes (north of, within, and south of the ACC). In the southernmost Weddell Sea, the 1/12° HYCOM model performed better than the 1/6° SOSE: separation of SOCCOM floats from both Argo floats and HYCOM simulated floats was less than 1,500 km after 2 years, while the SOSE prediction was much larger. Even though we are working with small numbers of floats, our simple dispersion estimate, based on growth of the distance between individual SOCCOM floats and the colocated Argo ensembles, is consistent with lateral diffusivity estimates in this region based on many more float pairs (Davis, 2005): highest in the Agulhas retroflection region north of the ACC, weaker in the ACC despite its mean flow, and smallest in the Weddell Sea. The largest differences between individual SOCCOM float trajectories and the ensembles resulted from frontal crossings.

The PS89 floats have sometimes been strongly guided by topographic features: Maud Rise, where the Weddell polynya (1974–1977) reopened coincidentally during our sampling period; the Agulhas Ridge and Spiess Seamount, which guide fronts, upwelling/mixing, and possibly outgassing; and the Southwest Indian Ridge, Crozet Plateau, and Kerguelen Plateau, which guide the primary ACC fronts. Some other brief findings worthy of expanded work include the process of upwelling and air-sea gas exchange in the ACC's Southern and Antarctic Zones where upwelled deep water is close to the sea surface, retention of water in

the Cape Basin in addition to its role as an Indian-Atlantic Ocean crossroads, low eddy energy in the Weddell Sea and nearly laminar current of the Antarctic Slope Front, and dispersion and prediction error of Argo floats as a function of mean and eddy kinetic energy.

As we move into the second half of SOCCOM, our deployment strategy has evolved to emphasize regions without coverage. Of highest priority are the Weddell Sea because of the failure to deploy in 2014–2015, the South Atlantic subtropical gyre, and the southwest and central Indian Ocean. In addition to the historical and SOSE-/HYCOM-simulated information, the trajectories and accumulating water property information from the ~100 existing SOCCOM floats are an invaluable asset for the remaining deployment strategy. With our growing fleet and increasing numbers of annual cycles, we are beginning to carry out more comprehensive, quantitative evaluations of our biogeochemical sampling coverage, which should inform planning for expansion to other regions.

As the biogeochemical profiling technology proves itself through these widespread Southern Ocean deployments, as well as expanding biogeochemical float programs in other nations, expansion to the global ocean is a natural segue (Biogeochemical-Argo Planning Group, 2016). These floats will transform our knowledge of ocean biogeochemistry—carbon, nutrients, oxygen, and net community production—to the same extent that core Argo has transformed study of the physical properties.

Acknowledgments

Support for SOCCOM observations was provided by NSF PLR-1425989, the international Argo Program, and the NOAA programs that contribute to it and NASA NNX14AP49G and NNX14AP496. J. W. acknowledges support from NSF OCE-1234473 and declares that this work was done as a private venture and not in the author's capacity as an employee of the Jet Propulsion Laboratory, California Institute of Technology. The UW Argo float lab, the MBARI float sensor group, and engineers at Seabird built and managed the SOCCOM floats and sensors. Chief Scientist Olaf Boebel and Mario Hoppema of the Alfred Wegener Institute led the Polarstern Expedition PS89 (ANT-XXX/2) and provided CTD/hydrographic data. Hannah Zanowski, SIO Shipboard Technical Support, and Andrew Dickson's lab at SIO collected and analyzed SOCCOM shipboard samples. A snapshot of the quality-controlled SOCCOM biogeochemical float data used in this study is available at http://doi.org/10.6075/J0QC01DJ. Data and graphics of float physical and most biogeochemical properties are available in near real time through the Coriolis database (http://www.ifremer.fr/co-argoFloats/). The float temperature and salinity data used in this project are available at http://doi.org/10.17882/42182 and were made freely available by the International Argo Program and the national programs that contribute to it. All data from Polarstern PS89 are archived at Pangaea (https://www.pangaea.de). Hydrographic data from the Polarstern PS89 cruise are available at https://cchdo.ucsd.edu/cruise/06AQ20141202. A table linking all PS89 SOCCOM calibration data sets is available at http://soccom.princeton.edu/content/status-tables. The WOCE Hydrographic Programme data set from 1992, Polarstern ANTX_4 (Chief Scientist P. Lemke) is available at https://cchdo.ucsd.edu/cruise/06AQANTX_4. Particle tracking in SOSE was carried out using the *Octopus* software developed by J. Wang (NASA JPL; http://github.com/jinbow/octopus/). Angelique Haza (RSMAS) performed the HYCOM simulations. Paul Chamberlain provided SOCCOM float plots.

References

Abernathey, R. P., Cerovecki, I., Holland, P., Newsom, E., Mazloff, M., & Talley, L. D. (2016). Water mass transformation by sea ice in the upper branch of the Southern Ocean overturning. *Nature Geoscience*, *9*, 596–601. https://doi.org/10.1038/ngeo2749

Ardyna, M., Claustre, H., Sallée, J.-B., D'Ovidio, F., Gentili, B., van Dijken, G., et al. (2017). Delineating environmental control of phytoplankton biomass and phenology in the Southern Ocean. *Geophysical Research Letters*, *44*, 5016–5024. https://doi.org/10.1002/2016GL072428

Arteaga, L., Haëntjens, N., Boss, E., Johnson, K. S., & Sarmiento, J. L. (2018). Assessment of export efficiency equations in the southern ocean applied to satellite-based net primary production. *Journal of Geophysical Research: Oceans*, *123*, 2945–2964. https://doi.org/10.1002/2018JC013787

Bakker, D. C. E., Hoppema, M., Schroder, M., Geibert, W., & deBaar H. J. W. (2008). A rapid transition from ice covered CO_2-rich waters to a biologically mediated CO_2 sink in the eastern Weddell Gyre. *Biogeosciences*, *5*, 1373–1386. https://doi.org/10.5194/bg-5-1373-2008

Balch, W. M., Drapeau, D. T., Bowler, B. C., Lyczskowski, E., Booth, E. S., & Alley, D. (2011). The contribution of coccolithophores to the optical and inorganic carbon budgets during the Southern Ocean Gas Exchange Experiment: New evidence in support of the "Great Calcite Belt" hypothesis. *Journal of Geophysical Research*, *116*, C00F06. https://doi.org/10.1029/2011JC006941

Bersch, M., Becker, G. A., Frey, H., & Koltermann, K. P. (1992). Topographic effects of the Maud Rise on the stratification and circulations of the Weddell Gyre. *Deep Sea Research*, *39*, 303–331.

Biogeochemical-Argo Planning Group (2016). In K. Johnson & H. Claustre (Eds.), *The scientific rationale, design and implementation plan for a biogeochemical-Argo float array*. https://doi.org/10.13155/46601

Bleck, R. (2002). An oceanic general circulation model framed in hybrid isopycnic-Cartesian coordinates. *Ocean Modelling*, *4*(1), 55–88. https://doi.org/10.1016/S1463-5003(01)00012-9

Boebel, O. (2015). The Expedition PS89 of the Research Vessel POLARSTERN to the Weddell Sea in 2014/2015, Berichte zur Polar- und Meeresforschung: *Reports on polar and marine research, Bremerhaven, Alfred Wegener Institute for Polar and Marine Research*, 689, 151 p.

Brandt, A., Bathmann, U., Brix, S., Cisewski, B., Flores, H., Göcke, C., et al. (2011). Maud Rise—A snapshot through the water column. *Deep-Sea Research Part II*, *58*(19-20), 1962–1982. https://doi.org/10.1016/j.dsr2.2011.01.008

Briggs, E., Martz, T. R., Talley, L. D., Mazloff, M. R., & Johnson, K. S. (2018). Physical and biological drivers of biogeochemical tracers within the seasonal ice zone of the Southern Ocean from profiling floats. *Journal of Geophysical Research: Oceans*, *123*, 746–758. https://doi.org/10.1002/2017JC012846

Bushinsky, S., Gray, A. R., Johnson, K. S., & Sarmiento, J. L. (2017). Oxygen in the Southern Ocean from Argo floats: Determination of processes driving air-sea fluxes. *Journal of Geophysical Research: Oceans*, *122*, 8661–8682. https://doi.org/10.1002/2017JC012923

Carranza, M. M., & Gille, S. T. (2015). Southern Ocean wind-driven entrainment enhances satellite chlorophyll-a through the summer. *Journal of Geophysical Research: Oceans*, *120*, 304–323. https://doi.org/10.1002/2014JC010203

Carter, B. R., Feely, R. A., Williams, N. L., Dickson, A. G., Fong, M. B., & Takeshita, Y. (2018). Updated methods for global locally interpolated estimation of alkalinity, pH, and nitrate. *Limnology and Oceanography: Methods*, *16*(2), 119–131. https://doi.org/10.1002/lom3.10232

Carter, B. R., Williams, N. L., Gray, A. R., & Feely, R. A. (2016). Locally interpolated alkalinity regression for global alkalinity estimation. *Limnology and Oceanography: Methods*, *14*, 268–277. https://doi.org/10.1002/lom3.10087

Cerovecki, I., Talley, L. D., & Mazloff, M. R. (2011). A comparison of Southern Ocean air-sea buoyancy flux from an ocean state estimate with five other products. *Journal of Climate*, *24*, 6283–6306.

Chamberlain, P., Talley, L. D., Mazloff, M., Riser, S., Speer, K., & Gray, A. R. (2018). Observing the ice covered Weddell Sea with profiling floats: Position uncertainties and correlation statistics. *Journal of Geophysical Research: Oceans*, *123*. https://doi.org/10.1029/2018JC014059

Chelton, D. B., Schlax, M. G., & Samelson, R. M. (2011). Global observations of nonlinear mesoscale eddies. *Progress in Oceanography*, *91*(2), 167–216. https://doi.org/10.1016/j.pocean.2011.01.002

Davis, R. E. (1991). Observing the general circulation with floats. *Deep-Sea Research*, *38*(Suppl), S531–S571.

Davis, R. E. (2005). Intermediate-depth circulation of the Indian and South Pacific Oceans measured by autonomous floats. *Journal of Physical Oceanography*, *35*, 683–707.

De Steur, L., Holland, D. M., Muench, R. D., & McPhee, M. G. (2007). The warm-water "Halo" around Maud Rise: Properties, dynamics and impact. *Deep-Sea Research Part I, 54,* 871–896. doi:https://doi.org/10.1016/j.dsr.2007.03.009

Ducet, N., Le Traon, P. Y., & Reverdin, G. (2000). Global high-resolution mapping of ocean circulation from TOPEX/Poseidon and ERS-1 and -2. *Journal of Geophysical Research*, *105*, 19,477–19,498.

Fahrbach, E., Hoppema, M., Rohardt, G., Boebel, O., Klatt, O., & Wisotzki, A. (2011). Warming of deep and abyssal water masses along the Greenwich meridian on decadal time scales: The Weddell gyre as a heat buffer. *Deep-Sea Research Part II*, *58*, 2509–2523.

Fay, A. R., & McKinley, G. A. (2014). Global ocean biomes: Mean and temporal variability. *Earth System Science Data*, *6*, 273–284. https://doi.org/10.5194/essd-6-273-2014

Freeland, H. J., Rhines, P. B., & Rossby, T. (1975). Statistical observations of the trajectories of neutrally buoyant floats in the North Atlantic. *Journal of Marine Research*, *33*, 383–404.

Frölicher, T. L., Sarmiento, J. L., Dunne, J. P., Kasting, J. P., & Winton, M. (2015). Dominance of the Southern Ocean in anthropogenic carbon and heat uptake in CMIP5 models. *Journal of Climate*, *28*, 862–886.

Garzoli, S. L., Dong, S., Fine, R., Meinen, C. S., Perez, R. C., Schmid, C., et al. (2015). The fate of the Deep Western Boundary Current in the South Atlantic. *Deep-Sea Research Part I*, *103*, 125–136. https://doi.org/10.1016/j.dsr.2015.05.008

Giglio, D., Lyubchich, V., & Mazloff, M. R. (2018). Estimating oxygen in the Southern Ocean using Argo temperature and salinity. *Journal of Geophysical Research: Oceans*, *123*, 4280–4297. https://doi.org/10.1029/2017JC013404

Gordon, A. L. (1978). Deep Antarctic convection west of Maud Rise. *Journal of Physical Oceanography*, *8*(4), 600–612. https://doi.org/10.1175/1520-0485(1978)008<0600:DACWOM>2.0.CO;2

Gordon, A. L. (2003). Oceanography: The brawniest retroflection. *Nature*, *421*(6,926), 904–905. https://doi.org/10.1038/421904a

Gordon, A. L., Visbeck, M., & Comiso, J. C. (2007). A possible link between the Weddell Polynya and the southern annular mode. *Journal of Climate*, *20*, 2558–2571. https://doi.org/10.1175/JCLI4046.1

Gray, A. L., Johnson, K. S., Bushinsky, S. M., Riser, S. C., Russell, J. L., Talley, L. D., et al. (2018). Autonomous biogeochemical floats detect significant carbon dioxide outgassing in the high-latitude Southern Ocean. *Geophysical Research Letters*, *45*, 9049–9057. https://doi.org/10.1029/2018GL078013

Haentjens, N., Boss, E., & Talley, L. D. (2017). Revisiting ocean color algorithms for chlorophyll a and particulate organic carbon in the Southern Ocean using biogeochemical floats. *Journal of Geophysical Research: Oceans*, *122*, 6583–6593. https://doi.org/10.1002/2017JC012844

Hanawa, K., & Talley, L. D. (2001). Mode waters. In G. Siedler, & J. Church (Eds.), *Ocean circulation and climate* (pp. 373–386). Academic Press: International Geophysics Series.

Haumann, F. A., Gruber, N., Münnich, M., Frenger, I., & Kern, S. (2016). Sea-ice transport driving Southern Ocean salinity and its recent trends. *Nature*, *537*, 89–92.

Holte, J., Talley, L., Gilson, J., & Roemmich, D. (2017). An Argo mixed layer climatology and data base. *Geophysical Research Letters*, *44*, 5618–5626. https://doi.org/10.1002/2017GL073426

Johnson, K. S., Plant, J. N., Coletti, L. J., Jannasch, H. W., Sakamoto, C. M., Riser, S. C., et al. (2017). Biogeochemical sensor performance in the SOCCOM profiling float array. *Journal of Geophysical Research: Oceans*, *122*, 6416–6436. https://doi.org/10.1002/2017JC012838

Johnson, K. S., Plant, J. N., Dunne, J. P., Talley, L. D., & Sarmiento, J. L. (2017). Annual nitrate drawdown observed by SOCCOM profiling floats and the relationship to annual net community production. *Journal of Geophysical Research: Oceans*, *122*, 6668–6683. https://doi.org/10.1002/2017JC012839

Kalnay, E., Kanamitsu, M., Kistler, R., Collins, W., Deaven, D., Gandin, L., et al. (1996). The NCEP-NCAR 40-year reanalysis project. *Bulletin of the American Meteorological Society*, *77*, 437–471.

Kamenkovich, I., Haza, A., Gray, A. R., Dufour, C. O., & Garraffo, Z. (2017). Observing System Simulation Experiments for an array of autonomous biogeochemical profiling floats in the Southern Ocean. *Journal of Geophysical Research: Oceans*, *122*, 7595–7611. https://doi.org/10.1002/2017JC012819

Khatiwala, S., Tanhua, T., Mikaloff Fletcher, S. E., Gerber, M., Doney, S. C., Graven, H. D., et al. (2013). Global ocean storage of anthropogenic carbon. *Biogeosciences*, *10*(4), 2169–2191. https://doi.org/10.5194/bg-10-2169-2013

Kim, Y. S., & Orsi, A. H. (2013). On the variability of Antarctic Circumpolar Current fronts inferred from 1992-2011 altimetry. *Journal of Physical Oceanography*, *44*, 3054–3071.

Klatt, O., Boebel, O., & Fahrbach, E. (2007). A profiling float's sense of ice. *Journal of Atmospheric and Oceanic Technology*, *24*, 1301–1308.

Klocker, A., Ferrari, R., LaCasce, J. H., & Merrifield, S. T. (2012). Reconciling float-based and tracer-based estimates of lateral diffusivities. *Journal of Marine Research*, *70*, 569–602. https://doi.org/10.1357/00222401280526743

Knust, R. (2014). Expedition Programme PS89, Expeditions Program Polarstern, Bremerhaven, Alfred Wegener Institute for Polar & Marine Research, PS89, 37 pp.

Koltermann, K. P., Gouretski, V. V., & Jancke, K. (2011). Hydrographic Atlas of the World Ocean Circulation Experiment (WOCE). Volume 3: Atlantic Ocean. In M. Sparrow, P. Chapman, & J. Gould (Eds.). Southampton, UK: International WOCE Project Office. Retrieved from http://whp-atlas.ucsd.edu/atlantic_index.html

LaCasce, J. H. (2008). Statistics from Lagrangian observations. *Progress in Oceanography*, *77*(1), 1–29. https://doi.org/10.1016/j.pocean.2008.02.002

Landschützer, P., Gruber, N., Bakker, D. C. E., & Schuster, U. (2014). Recent variability of the global ocean carbon sink. *Global Biogeochemical Cycles*, *28*, 927–949. https://doi.org/10.1002/2014GB004853

Large, W. G., & Yeager, S. G. (2009). The global climatology of an interannually varying air–sea flux data set. *Climate Dynamics*, *33*(2-3), 341–364. https://doi.org/10.1007/s00382-008-0441-3

Ledwell, J. R., Laurent, L. C. S., Girton, J. B., & Toole, J. M. (2011). Diapycnal mixing in the Antarctic Circumpolar Current. *Journal of Physical Oceanography*, *41*, 241–246. https://doi.org/10.1175/2010jpo4557.1

Liang, Y. C., Mazloff, M. R., Rosso, I., Fang, S. W., & Yu, J. Y. (2018). A multi-variate empirical orthogonal function method to construct nitrate maps in the Southern Ocean. *Journal of Atmospheric and Oceanic Technology*, *35*, 1505–1519. https://doi.org/10.1175/JTECH-D-18-0018.1

Lumpkin, R., & Johnson, G. C. (2013). Global ocean surface velocities from drifters: Mean, variance, El Nino–Southern Oscillation response, and seasonal cycle. *Journal of Geophysical Research: Oceans*, *118*, 2992–3006. https://doi.org/10.1002/jgrc.20210

Majkut, J. D., Carter, B. R., Frölicher, T. L., Dufour, C. O., Rodgers, K. B., & Sarmiento, J. L. (2014). An observing system simulation for Southern Ocean carbon dioxide uptake. *Philosophical Transactions of the Royal Society A*, *372*, 20130046. https://doi.org/10.1098/rsta.2013.0046

Marshall, J., & Speer, K. (2012). Closure of the meridional overturning circulation through Southern Ocean upwelling. *Nature Geoscience*, *5*, 171–180. https://doi.org/10.1038/ngeo1391

Martinson, D. G., Killworth, P. D., & Gordon, A. L. (1981). A convective model for the Weddell Polynya. *Journal of Physical Oceanography*, *11*(4), 466–488. https://doi.org/10.1175/1520-0485(1981)011<0466:ACMFTW>2.0.CO;2

Masich, J., Chereskin, T. K., & Mazloff, M. R. (2015). Topographic form stress in the Southern Ocean state estimate. *Journal of Geophysical Research: Oceans*, *120*, 7919–7933. https://doi.org/10.1002/2015JC011143

Maslanik, J., & Stroeve, J. (1999). *Near-real-time DMSP SSMIS daily polar gridded sea ice concentrations, version 1*. (Indicate subset used). Boulder, Colorado USA: NASA National Snow and Ice Data Center Distributed Active Archive Center. Retrieved from https://doi.org/10.5067/U8C09DWVX9LM. (Date Accessed)

Mazloff, M. R., Cornuelle, B. D., Gille, S. T., & Verdy, A. (2018). Correlation lengths for estimating the large-scale carbon and heat content of the Southern Ocean. *Journal of Geophysical Research: Oceans*, *123*, 883–901. https://doi.org/10.1002/2017JC013408

Mazloff, M. R., Heimbach, P., & Wunsch, C. (2010). An eddy-permitting Southern Ocean State Estimate. *Journal of Physical Oceanography*, *40*, 880–899.

McCartney, M. S. (1982). The subtropical circulation of mode waters. *Journal of Marine Research*, *40*(Suppl), 427–464.

Moore, J. K., & Abbott, M. R. (2000). Phytoplanton chlorophyll distributions and primary production in the Southern Ocean. *Journal of Geophysical Research*, *105*(C12), 28,709–28,722. https://doi.org/10.1029/1999JC000043

Muench, R. D., Morison, J. H., Padman, L., Martinson, D., Schlosser, P., Huber, B., & et al. (2001). Maud Rise revisited. *Journal of Geophysical Research*, *106*(C2), 2423–2440. https://doi.org/10.1029/2000JC000531

Naveira Garabato, A. C., Jullion, L., Stevens, D. P., Heywood, K. J., & King, B. A. (2009). Variability of subantarctic mode water and Antarctic intermediate water in the Drake Passage during the late twentieth and early twenty-first century. *Journal of Climate*, *22*, 3661–3688. https://doi.org/10.1175/2009JCLI2621.1

Naveira Garabato, A. C., Polzin, K. L., Ferrari, R., Zika, J. D., & Forryan, A. (2016). A microscale view of mixing and overturning across the Antarctic Circumpolar Current. *Journal of Physical Oceanography*, *46*, 233–254. https://doi.org/10.1175/jpo-d-15-0025.1

Naveira Garabato, A. C., Polzin, K. L., King, B. A., Heywood, K. J., & Visbeck, M. (2004). Widespread intense turbulent mixing in the Southern Ocean. *Science*, *303*, 210–213. https://doi.org/10.1126/science.1090929

Ohshima, K. I., Fukamachi, Y., Williams, G. D., Nihashi, S., Roquet, F., Kitade, Y., et al. (2013). Antarctic Bottom Water production by intense sea-ice formation in the Cape Darnley polynya. *Nature Geoscience*, *6*, 235–240. https://doi.org/10.1038/ngeo1738

Olsen, A., Key, R. M., van Heuven, S., Lauvset, S. K., Velo, A., Lin, X., et al. (2016). The Global Ocean Data Analysis Project version 2 (GLODAPv2)—An internally consistent data product for the world ocean. *Earth System Science Data*, *8*, 297–323. https://doi.org/10.5194/essd-8-297-2016

Orsi, A. H., Nowlin, W. D., & Whitworth, T. (1993). On the circulation and stratification of the Weddell Gyre. *Deep-Sea Research Part I*, *40*(1), 169–203. https://doi.org/10.1016/0967-0637(93)90060-G

Orsi, A. H., & Whitworth, T. (2005). Hydrographic Atlas of the World Ocean Circulation Experiment (WOCE). Volume 1: Southern Ocean. In M. Sparrow, P. Chapman & J. Gould (Eds.). Southampton, UK. International WOCE Project Office. Retrieved from http://woceatlas.tamu.edu/index.html

Orsi, A. H., Whitworth, T., & Nowlin, W. D. (1995). On the meridional extent and fronts of the Antarctic circumpolar current. *Deep-Sea Research Part I*, *42*, 641–673.

Ou, H. W. (1991). Some effects of a seamount on oceanic flows. *Journal of Physical Oceanography*, *21*, 1835–1845.

Poteau, A., Boss, E., & Claustre, H. (2017). Particulate concentration and seasonal dynamics in the mesopelagic ocean based on the back-scattering coefficient measured with biogeochemical-Argo floats. *Geophysical Research Letters*, *44*, 6933–6939. https://doi.org/10.1002/2017GL073949

Purkey, S. G., & Johnson, G. C. (2010). Warming of global abyssal and deep Southern Ocean waters between the 1990s and 2000s: Contributions to global heat and sea level rise budgets. *Journal of Climate*, *23*, 6336–6351.

Purkey, S. G., & Johnson, G. C. (2013). Antarctic Bottom Water warming and freshening: Contributions to sea level rise, ocean freshwater budgets, and global heat gain. *Journal of Climate*, *26*, 6106–6122.

Reid, J. L. (1994). On the total geostrophic circulation of the North-Atlantic Ocean: Flow patterns, tracers, and transports. *Progress in Oceanography*, *33*, 1–92.

Reid, J. L. (2003). On the total geostrophic circulation of the Indian Ocean: Flow patterns, tracers and transports. *Progress in Oceanography*, *56*, 137–186.

Rhein, M., Rintoul, S. R., Aoki, S., Campos, E., Chambers, D., Feely, R. A., et al. (2013). Observations: Ocean. In T. F. Stocker, D. Qin, G.-K. Plattner, M. Tignor, S. K. Allen, J. Boschung, et al. (Eds.), *Climate Change 2013: The Physical Science Basis. Contribution of Working Group I to the Fifth Assessment Report of the Intergovernmental Panel on Climate Change* (pp. 255–315). Cambridge, United Kingdom and New York, NY, USA: Cambridge University Press.

Richardson, P. L. (2007). Agulhas leakage into the Atlantic estimated with subsurface floats and surface drifters. *Deep-Sea Research Part I*, *54*(8), 1361–1389. https://doi.org/10.1016/j.dsr.2007.04.010

Riser, S., Freeland, H., Roemmich, D., Wijffels, S., Troisi, A., Belbeoch, M., et al. (2016). Fifteen years of observations with the global Argo array. *Nature Climate Change*, *6*, 145–153. https://doi.org/10.1038/NCLIMATE2872

Riser, S. C. (1982). The quasi-Lagrangian nature of SOFAR floats. *Deep Sea Research*, *29*(12), 1587–1602. https://doi.org/10.1016/0198-0149(82)90045-0

Riser, S. C., Swift, D., & Drucker, R. (2018). Profiling floats in SOCCOM: Technical capabilities for studying the Southern Ocean. *Journal of Geophysical Research: Oceans*, *123*, 4055–4073. https://doi.org/10.1002/2017JC013419

Roemmich, D., Johnson, G. C., Riser, S., Davis, R., Gilson, J., Owens, W. B., et al. (2009). The Argo program: Observing the global ocean with profiling floats. *Oceanography*, *22*, 34–43. https://doi.org/10.5670/oceanog.2009.36

Rosso, I., Mazloff, M. R., Verdy, A., & Talley, L. D. (2017). Space and time variability of the Southern Ocean carbon budget. *Journal of Geophysical Research: Oceans*, *122*, 7407–7432. https://doi.org/10.1002/2016JC012646

Russell, J., Kamenkovich, I., Bitz, C., Ferrari, R., Gille, S. T., Goodman, P. J., et al. (2018). Metrics for the evaluation of the Southern Ocean in Coupled Climate Models and Earth System Models. *Journal of Geophysical Research: Oceans*, *123*, 3120–3143. https://doi.org/10.1002/2017JC013461

Sallée, J.-B., Speer, K., Rintoul, S., & Wijffels, S. (2010). Southern Ocean thermocline ventilation. *Journal of Physical Oceanography*, *40*(3), 509–529. https://doi.org/10.1175/2009JPO4291.1

Sallée, J.-B., Speer, K. G., & Rintoul, S. R. (2010). Zonally asymmetric response of the Southern Ocean mixed-layer depth to the Southern Annular Mode. *Nature Geoscience*, *3*(4), 273–279. https://doi.org/10.1038/ngeo812

Sarmiento, J. L., Gruber, N., Brzezinski, M. A., & Dunne, J. P. (2004). High-latitude controls of thermocline nutrients and low latitude biological productivity. *Nature*, *427*, 5465–5480. https://doi.org/10.1038/nature02127

Smith, W. H. F., & Sandwell, D. T. (1997). Global seafloor topography from satellite altimetry and ship depth soundings. *Science*, *277*, 1957–1962.

Sokolov, S., & Rintoul, S. R. (2009). Circumpolar structure and distribution of the Antarctic Circumpolar Current fronts: 1. Mean circumpolar paths. *Journal of Geophysical Research*, *114*, C11018. https://doi.org/10.1029/2008JC005108

Speer, K., Rintoul, S. R., & Sloyan, B. (2000). The diabatic Deacon cell. *Journal of Physical Oceanography*, *30*(12), 3212–3222. https://doi.org/10.1175/1520-0485(2000)030<3212:TDDC>2.0.CO;2

Suga, T., & Talley, L. D. (1995). Antarctic Intermediate Water circulation in the tropical and subtropical South Atlantic. *Journal of Geophysical Research*, *100*(C7), 13,441–13,453. https://doi.org/10.1029/95JC00858

Swart, S., Campbell, E. C., Heuze, C. H., Johnson, K., Lieser, J. L., Massom, R., et al. (2018). Return of the Maud Rise polynya: Climate litmus or sea ice anomaly? [in "State of the Climate in 2017"]. *Bulletin of the American Meteorological Society*, *99*, S188–S189. https://doi.org/10.11756/2018BAMSStateoftheClimate.I

Takahashi, T., Sutherland, S. C., Wanninkhof, R., Sweeney, C., Feely, R. A., Chipman, D. W., et al. (2009). Climatological mean and decadal change in surface ocean pCO_2 and net sea–air CO_2 flux over the global oceans. *Deep Sea Research*, *II*(56), 554–577.

Talley, L. D. (1996). Antarctic Intermediate Water in the South Atlantic. In G. Wefer, W. H. Berger, G. Siedler, & D. Webb (Eds.), *The South Atlantic: Present and past circulation* (pp. 219–238). Berlin: Springer-Verlag.

Talley, L. D. (2013). Closure of the global overturning circulation through the Indian, Pacific and Southern Oceans: Schematics and transports. *Oceanography*, *26*, 80–97. https://doi.org/10.5670/oceanog.2013.07

Talley, L. D., Becker, S., Key, R., Dickson, A., Boss, E., & Sakamoto, C. (2017). SOCCOM BGC floats: shipboard calibration data requirements. https://soccom.princeton.edu/sites/default/files/media/pdf/SOCCOM%20shipboard_data_manual_8jan2017.pdf, accessed 27 Feb. 2017

Talley, L. D., Feely, R. A., Sloyan, B. M., Wanninkhof, R., Baringer, M. O., Bullister, J. L., et al. (2016). Changes in ocean heat, carbon content, and ventilation: Review of the first decade of global repeat hydrography (GO-SHIP). *Annual Review of Marine Science*, *8*(1), 185–215. https://doi.org/10.1146/annurev-marine-052915-100829

Talley, L. D., Johnson, K., Riser, S., Boss, E., Schuller, D., Dickson, A., & et al. (2015). SOCCOM biogeochemical profiling float deployments from Polarstern PS89 (ANT-X/2). SOCCOM Tech. Rep.2015–1. Retrieved from http://soccom.princeton.edu/sites/default/files/files/SOCCOM_2015-1_PS89_floats.pdf

Talley, L. D., Pickard, G. L., Emery, W. J., & Swift, J. H. (2011). *Descriptive physical oceanography: An introduction*, (Sixth ed.). Boston, MA: Elsevier.

Tamsitt, V., Drake, H., Morrison, A. K., Talley, L. D., Dufour, C. O., Gray, A. R., et al. (2017). Spiraling up: Pathways of global deep waters to the surface of the Southern Ocean. *Nature Communications*, *8*(1), 1–10. https://doi.org/10.1038/s41467-017-00197-0

Tamsitt, V., Talley, L. D., Mazloff, M. R., & Cerovecki, I. (2016). Zonal variations in the Southern Ocean heat budget. *Journal of Climate*, *29*, 6563–6579.

Thompson, A. F., & Naveira Garabato, A. C. (2014). Equilibration of the Antarctic Circumpolar Current by standing meanders. *Journal of Physical Oceanography*, *44*, 1811–1828. https://doi.org/10.1175/JPO-D-13-0163.1

Thompson, A. F., & Sallée, J. B. (2012). Jets and topography: Jet transitions and the impact on transport in the Antarctic Circumpolar Current. *Journal of Physical Oceanography*, *42*(6), 956–972. https://doi.org/10.1175/JPO-D-11-0135.1

Tsuchiya, M., Talley, L. D., & McCartney, M. S. (1994). Water mass distributions in the western Atlantic: A section from South Georgia Island (54S) northward across the equator. *Journal of Marine Research*, *52*, 55–81.

Van Sebille, E., Griffies, S. M., Abernathey, R., Adams, T. P., Berloff, P., Biastoch, A., et al. (2018). Lagrangian ocean analysis: Fundamentals and practices. *Ocean Modelling*, *121*, 49–75. https://doi.org/10.1016/j.ocemod.2017.11.008

Van Sebille, E., Johns, W. E., & Beal, L. M. (2012). Does the vorticity flux from Agulhas rings control the zonal pathway of NADW across the South Atlantic? *Journal of Geophysical Research*, *117*, C05037. https://doi.org/10.1029/2011JC007684

Verdy, A., & Mazloff, M. R. (2017). A data assimilating model for estimating Southern Ocean biogeochemistry. *Journal of Geophysical Research: Oceans*, *122*, 6968–6988. https://doi.org/10.1002/2016JC012650

Wang, T., Gille, S. T., Mazloff, M. R., Zilberman, N. V., & Du, Y. (2018). Numerical simulations to project Argo float positions in the mid-depth and deep southwest Pacific. *Journal of Atmospheric and Oceanic Technology*, *35*, 1425–1440. https://doi.org/10.1175/JTECH-D-17-0214.1

Weijer, W., Veneziani, M., Stössel, A., Hecht, M. W., Jeffery, N., Jonko, A., et al. (2017). Local atmospheric response to an open-ocean polynya in a high-resolution climate model. *Journal of Climate*, *30*(5), 1629–1641. https://doi.org/10.1175/JCLI-D-16-0120.1

Williams, N. L., Juranek, L. W., Feely, R. A., Johnson, K. S., Sarmiento, J. L., Talley, L. D., et al. (2017). Calculating surface ocean pCO_2 flux from biogeochemical Argo floats equipped with pH: An uncertainty analysis. *Global Biogeochemical Cycles*, *31*, 591–604. https://doi.org/10.1002/2016GB005541

Williams, N. L., Juranek, L. W., Feely, R. A., Russell, J. L., Johnson, K. S., & Hales, B. (2018). Assessment of the carbonate chemistry seasonal cycles in the Southern Ocean from persistent observational platforms. *Journal of Geophysical Research: Oceans*, *123*, 4833–4852. https://doi.org/10.1029/2017JC012917

Williams, N. L., Juranek, L. W., Johnson, K. S., Feely, R. A., Riser, S. C., Talley, L. D., et al. (2016). Empirical algorithms to estimate water column pH in the Southern Ocean. *Geophysical Research Letters*, *43*, 3415–3422. https://doi.org/10.1002/2016GL068539

Wong, A. P., & Riser, S. C. (2011). Profiling float observations of the upper ocean under sea ice off the Wilkes Land Coast of Antarctica. *Journal of Physical Oceanography*, *41*, 1102–1115.

Wunsch, C., & Heimbach, P. (2007). Practical global oceanic state estimation. *Physica D*, *230*, 197–208. https://doi.org/10.1016/j.physd.2006.09.040

Zhurbas, V., & Oh, I. S. (2004). Drifter-derived maps of lateral diffusivity in the Pacific and Atlantic Oceans in relation to surface circulation patterns. *Journal of Geophysical Research*, *109*, C05015. https://doi.org/10.1029/2003JC002241